

# Support Information

## Phase distribution, deposition, and precipitation scavenging of atmospheric semi-volatile organic compounds under steady-state partitioning theory

Pu-Fei Yang<sup>1,2,3,4</sup>, Wan-Li Ma<sup>1,2,3</sup>, Zi-Feng Zhang<sup>1,2,3</sup>, Li-Yan Liu<sup>1,2,3</sup>, Hang Xiao<sup>5,6</sup>, Kaj Mantzius Hansen<sup>4</sup>, Hong-Liang Jia<sup>7</sup>, Li Li<sup>8</sup>, Peng-Tuan Hu<sup>9</sup>, Roland Kallenborn<sup>10</sup>, Yi-Fan Li<sup>1,7,11,12\*</sup>

<sup>1</sup>International Joint Research Center for Persistent Toxic Substances (IJRC-PTS), State Key Laboratory of Urban Water Resource and Environment, Harbin Institute of Technology, Harbin 150090, China

<sup>2</sup>International Joint Research Center for Arctic Environment and Ecosystem (IJRC-AEE), Polar Academy, Harbin Institute of Technology (PA-HIT), Harbin 150090, China

<sup>3</sup>Heilongjiang Provincial Key Laboratory of Polar Environment and Ecosystem (HPKL-PEE), Harbin 150090, China

<sup>4</sup>Department of Environmental Science, Aarhus University, Roskilde 4000, Denmark

<sup>5</sup>Key Laboratory of Urban Environment and Health, Ningbo Observation and Research Station, Institute of Urban Environment, Chinese Academy of Sciences, Xiamen 361021, China

<sup>6</sup>Zhejiang Key Laboratory of Urban Environmental Processes and Pollution Control, CAS Haixi Industrial Technology Innovation Center in Beilun, Ningbo 315830, China

<sup>7</sup>IJRC-PTS, College of Environmental Science and Engineering, Dalian Maritime University, Dalian 116026, China

<sup>8</sup>School of Public Health, University of Nevada, Reno, Reno, NV 89557, USA

<sup>9</sup>IJRC-PTS, Henan Normal University, XinXiang 453007, Henan, China

<sup>10</sup>Faculty of Chemistry, Biotechnology and Food Science (KBM), Norwegian University of Life Science, Norway

<sup>11</sup>IJRC-PTS, Green & Low Carbon Planning Institute (GLoCPI), Kunming, 650217, China

<sup>12</sup>IJRC-PTS-NA, Toronto, ON, M2J 3N8, Canada

\* Correspondence: Yi-Fan Li, International Joint Research Center for Persistent Toxic Substances (IJRC-PTS), State Key Laboratory of Urban Water Resource and Environment, Harbin Institute of Technology, Harbin 150090, China. Email: dr\_li\_yifan@163.com

**Number of pages: 52; Number of figures: 12; Number of tables: 6**

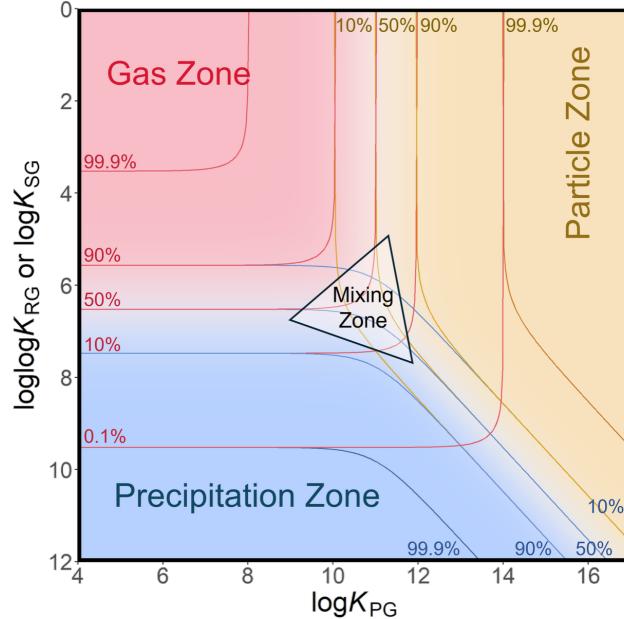
Figures.....	4
Figure S1 Schematic diagrams of distribution CSM and deposition CSM.....	4
Figure S2 Steps to place the OCPs in the CSMs.....	7
Figure S3 Steps to place the PCBs in the CSMs.....	10
Figure S4 Steps to place the PAHs in the CSMs.....	13
Figure S5 Steps to place the PBDEs in the CSMs .....	16
Figure S6 $\log K_{PG}$ , $\log K_{RG}$ , and $\log K_{SG}$ for four selected SVOCs as functions of temperature .....	19
Figure S7 Sensitivity analysis of TSP on distribution.....	20
Figure S8 Sensitivity analysis of TSP on deposition .....	21
Figure S9 Sensitivity analysis of TSP on scavenging .....	22
Figure S10 Sensitivity analysis of precipitation rate on distribution .....	23
Figure S11 Sensitivity analysis of precipitation rate on deposition .....	24
Figure S12 Result of BETR-Global: normalized global air concentration of CB-180.....	25
Tables .....	26
Table S1 Nomenclature and default values .....	26
Table S2 Physical-chemical properties and measurements for 36 selected chemicals.....	29
Table S3 The type categories of the 36 chemicals for the temperature above and below the freezing point.....	32
Table S4 Sensitivity (slope of linear regression) of 4-types SVOCs' $\Phi$ , $\Psi$ , and $W$ on TSP and precipitation rates .....	33
Table S5 Annual total deposition flux of BDE-209 from 2008 to 2009 in 10 Chinese cities (E: equilibrium; S: steady-state). ....	34
Table S6 Comparison between equilibrium models and steady-state models in this study .....	35
Text.....	36
Text S1 Clarification of some concepts about partition ratio.....	36
Text S1.1 Particle-gas partition ratio.....	36
Text S1.2 Rain-gas partition ratio and snow-gas partition ratio.....	36
Text S2 Relationship between $v_P$ and TSP, $v_W$ and $U_w$ .....	37

Text S3 Fugacity based methods calculations.....	38
Text S3.1 Z values.....	38
Text S3.2 <i>D</i> values for atmospheric chemicals deposition.....	38
Text S3.3 Chemical diffusion between gas and other phases: the mass transfer coefficients (MTCs).....	39
Text S3.4 Steady-state derivation.....	40
Text S4 Uncertainty and sensitivity analysis.....	42
Text S4.1 Uncertainty analysis for $\alpha_R$ and $\alpha_S$ .....	42
Text S4.2 Sensitivity analysis for $\Phi$ , $\Psi$ , and $W$ .....	42
Text S4.3 Discussion on unquantified uncertainty factors.....	43
Text S5 Methods of case studies .....	45
Text S5.1 OECD POV & LRTP Screening Tool on $\beta$ -HCH .....	45
Text S5.2 BETR Global V2.0 model.....	45
Text S5.3 Calculation of BDE-209's annual total deposition .....	45
Text S6 Vapor pressure based and octanol-air based absorptive partitioning approaches.....	47
Text S6.1 Junge-Pankow model.....	47
Text S6.2 Harner-Bidleman model.....	48
Text S6.3 Comparison between pressure based and octanol-air based absorptive partitioning equations .....	48
Reference.....	49

## Figures

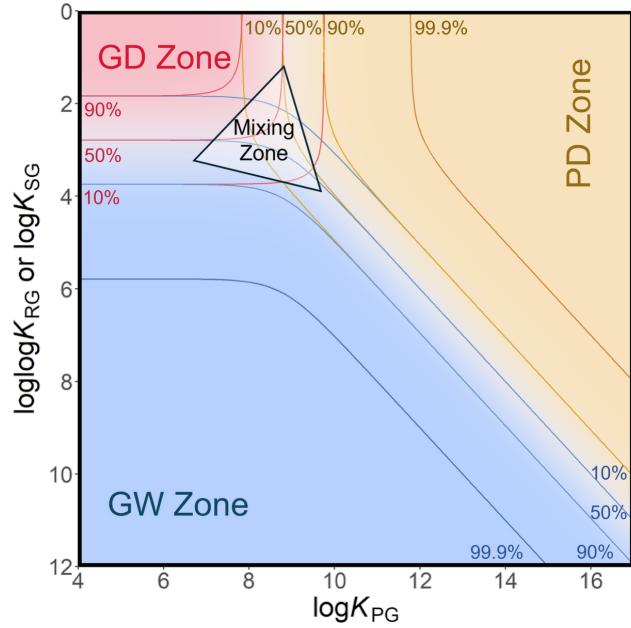
**Figure S1** Schematic diagrams of distribution CSM and deposition CSM.

(a)



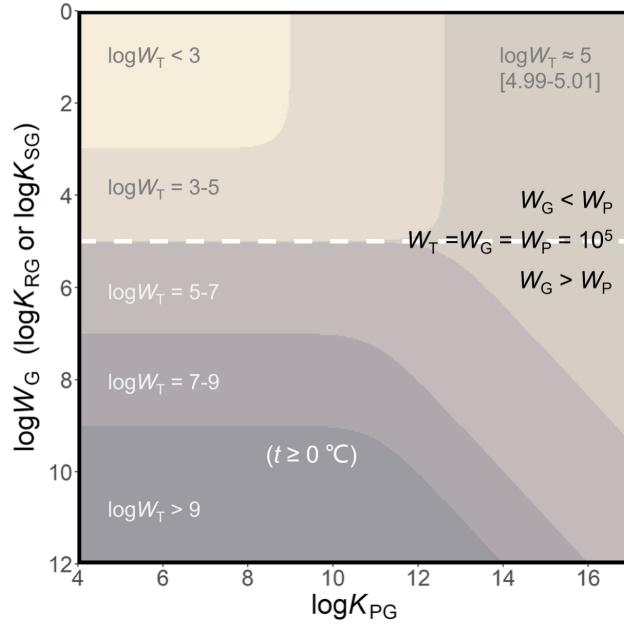
Schematic diagrams of distribution CSM. The distribution fraction  $\Phi$  is shown as colors in the background (red: for gas,  $\Phi_G$ , yellow: for particle  $\Phi_P$ , and blue: for rain or snow,  $\Phi_R/\Phi_S$ ), and darker colors represent higher  $\Phi$  values. There are also several auxiliary lines with different colors and percentages nearby, forming the ranges and zones of the  $\Phi$  values. There are three zones in each distribution CSM. The pink area in the upper left corner, the yellow area in the upper right corner and the blue area in the lower left are the Gas Zone, the Particle Zone and the Precipitation Zone, respectively. The precipitation zone is also called the Rain Zone when  $t \geq 0$  °C and the Snow Zone when  $t < 0$  °C. These three zones are bounded by the lines of the 50% of the chemicals in the phase represented by the zones. There is a near-triangle region in the center of the CSMs outside all of the three Zones, called the Mixing Zone, in which the SVOCs that are found in all the three phase in the atmosphere in noticeable fractions (<50% and >10%).

(b)



Schematic diagrams of deposition CSM. The background colors and auxiliary lines (red: for gaseous dry deposition,  $\Psi_{GDD}$ ; yellow: for particular dry and wet deposition,  $\Psi_{PDD} + \Psi_{PWD}$ ; and blue: gaseous wet deposition,  $\Psi_{GWD}$ ). The numbers along these lines are the  $\Psi$  values of the SVOCs calculated using equations in Table 1, forming the ranges and zones of the  $\Psi$  values. There are also three zones. The zone of gaseous dry deposition (GD zone), the zone of gaseous wet deposition (GW Zone), and the zone of particulate deposition (PD Zone) are also all bounded by the 50% contributions from each deposition category. The Mixing Zone located in the center of the deposition CSMs, in which appreciable deposition contributions (>10%) of the SVOCs are found for all the three categories in the atmosphere.

(c)

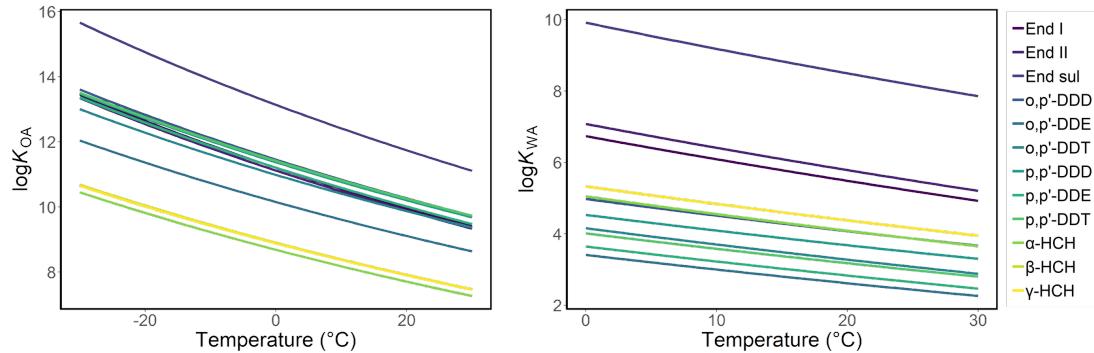


Schematic diagrams of scavenging CSM. Different from  $\Phi$  CSMs and  $\Psi$  CSMs, a  $W$  CSM only display  $W_T$ . In a  $W$  CSM, the range of  $\log W_T$  is grouped into six intervals:  $(0, 3)$ ,  $[3, 4.99]$ ,  $[4.99, 5.01]$ ,  $(5.01, 7)$ ,  $[7, 9]$ , and  $[9, \text{Inf}]$ . The white dashed lines split the  $W$  CSM into two zones. In the upper zone,  $W_G < W_P = 10^5$ ,  $W_T$  increases as  $\log K_{PG}$  increases. On the dashed line,  $W_G = W_P = 10^5$ ,  $W_T$  is a constant as  $\log K_{PG}$  changes. In the below zone,  $W_G > W_P = 10^5$ ,  $W_T$  decreases as  $\log K_{PG}$  increases.

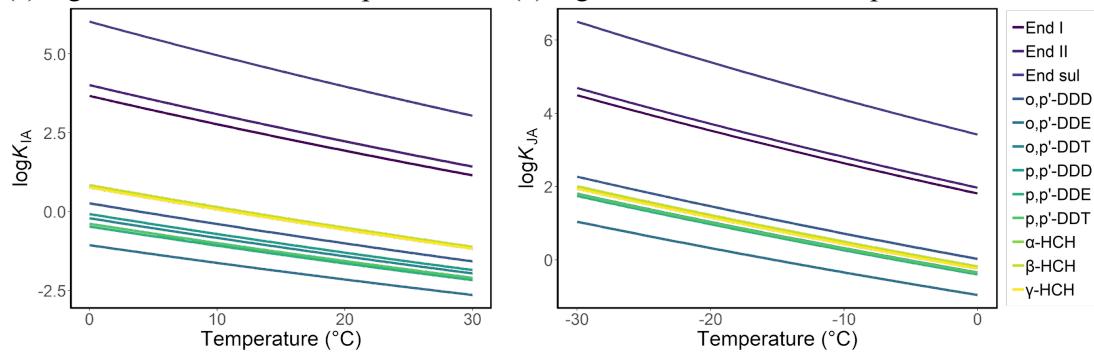
## Figure S2 Steps to place the OCPs in the CSMs

*Step 1 Calculate log $K_{OA}$ , log $K_{WA}$ , log $K_{IA}$ , and log $K_{JA}$  as functions of temperature*

(a) log $K_{OA}$  as a function of temperature. (b) log $K_{WA}$  as a function of temperature.



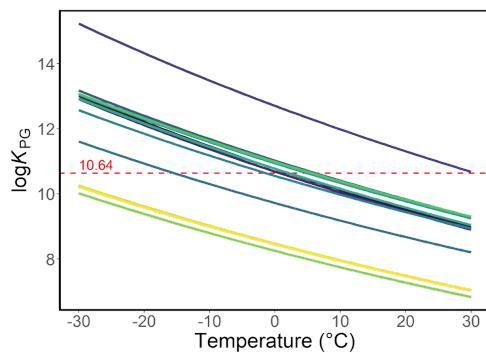
(c) log $K_{IA}$  as a function of temperature.



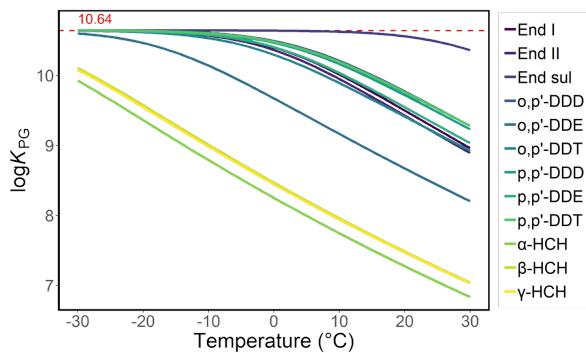
*Step 2 Calculate logK<sub>PG</sub>, logK<sub>RG</sub>, and logK<sub>SG</sub> as functions of temperature*

(e) logK<sub>PG</sub> as a function of temperature.

Equilibrium

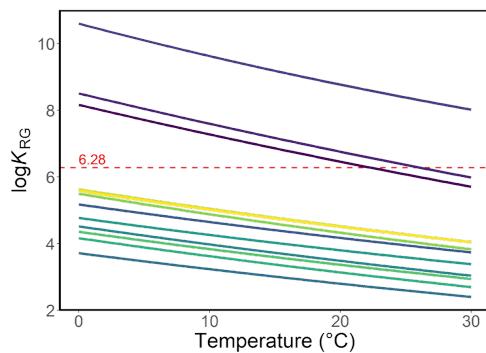


Steady-state

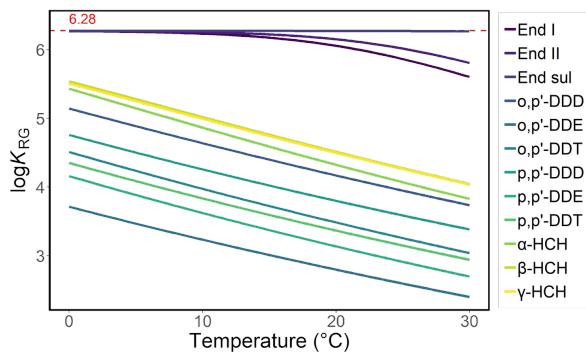


(f) logK<sub>RG</sub> as a function of temperature.

Equilibrium

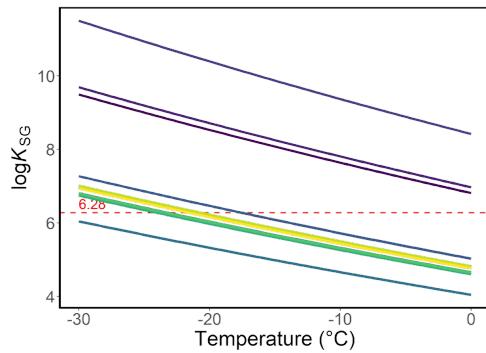


Steady-state

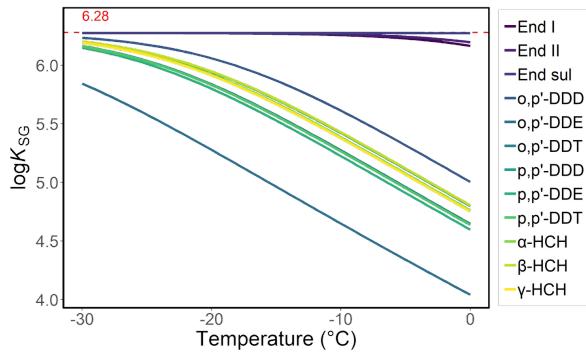


(g) logK<sub>SG</sub> as a function of temperature.

Equilibrium

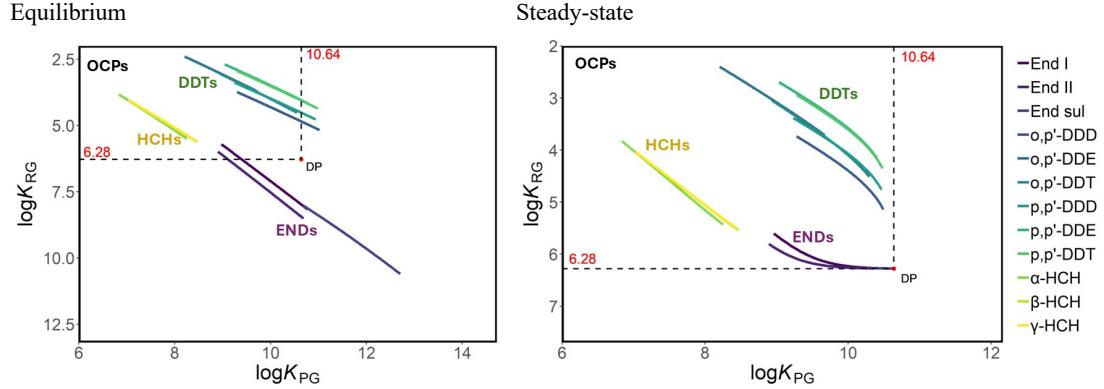


Steady-state

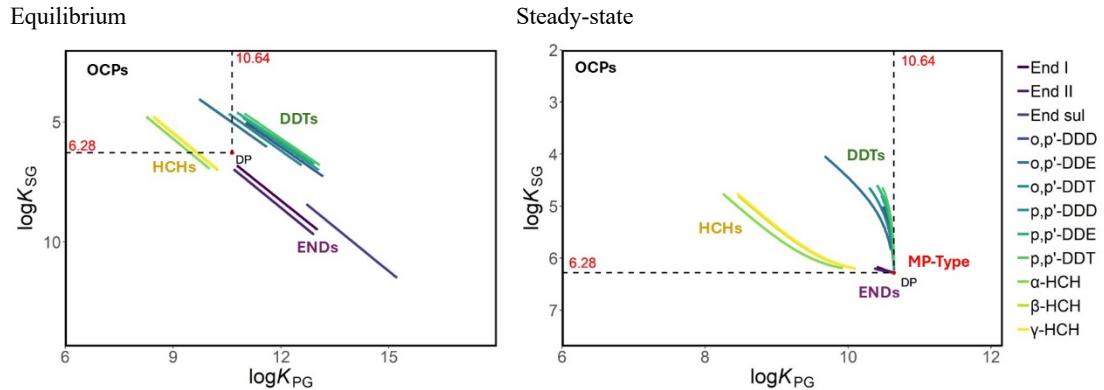


*Step 3 Plot log $K_{PG}$  and log $K_{RG}$  (log $K_{SG}$ ) at the same temperature as x and y axes*

(h) log $K_{RG}$  as a function of log $K_{PG}$ . CSMs when  $t \geq 0$  °C.



(i) log $K_{SG}$  as a function of log $K_{PG}$ . CSMs when  $t < 0$  °C.

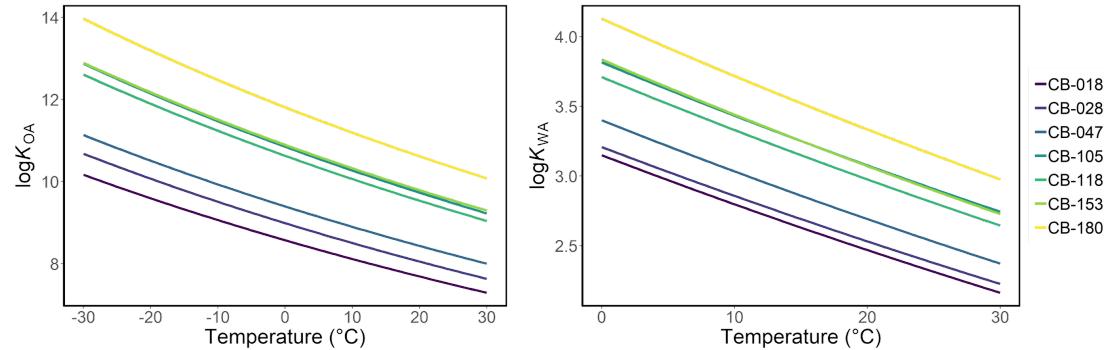


Parameters for 12 selected OCPs. log $K_{OA}$  (a), log $K_{WA}$  (b), log $K_{IA}$  (c), and log $K_{JA}$  (d) as functions of temperature. log $K_{PG}$  (e), log $K_{RG}$  (f), and log $K_{SG}$  (g) as functions of temperature. log $K_{RG}$  (h) and log $K_{RG}$  (i) as functions of log $K_{PG}$ . The left panels are from equilibrium equations, and the right panels are from steady-state equations.

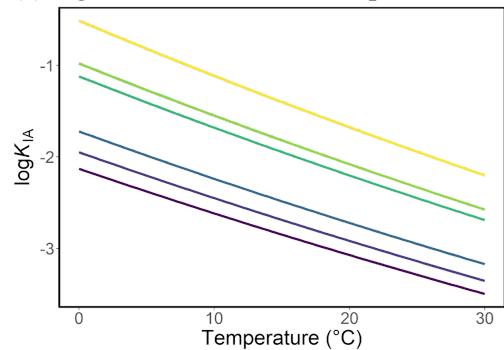
**Figure S3** Steps to place the PCBs in the CSMs

*Step 1 Calculate  $\log K_{OA}$ ,  $\log K_{WA}$ ,  $\log K_{IA}$ , and  $\log K_{JA}$  as functions of temperature*

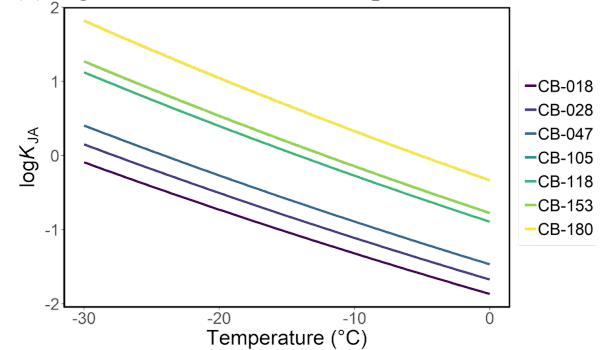
(a)  $\log K_{OA}$  as a function of temperature. (b)  $\log K_{WA}$  as a function of temperature.



(c)  $\log K_{IA}$  as a function of temperature.



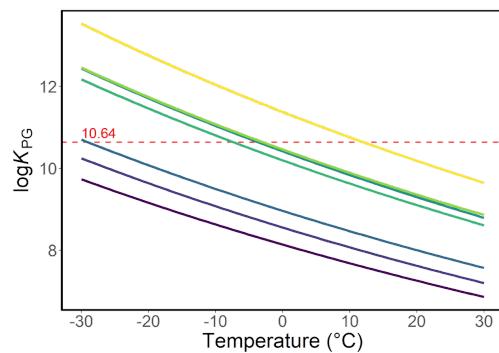
(d)  $\log K_{JA}$  as a function of temperature.



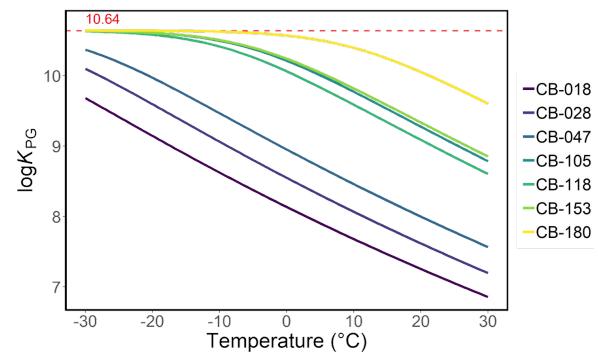
*Step 2 Calculate logK<sub>PG</sub>, logK<sub>RG</sub>, and logK<sub>SG</sub> as functions of temperature*

(e) logK<sub>PG</sub> as a function of temperature.

Equilibrium

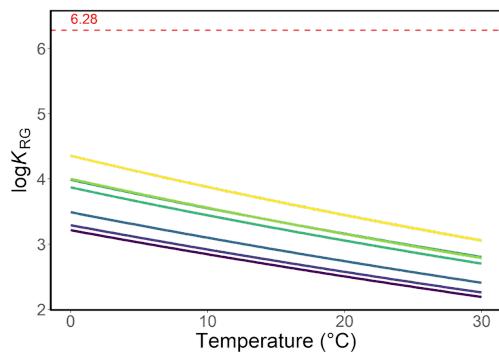


Steady-state

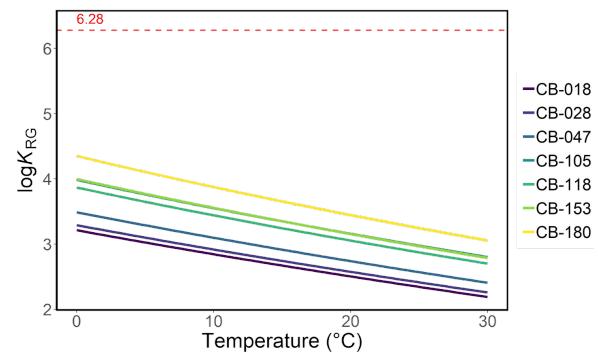


(f) logK<sub>RG</sub> as a function of temperature.

Equilibrium

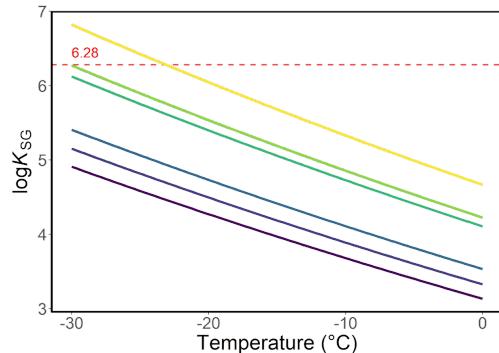


Steady-state

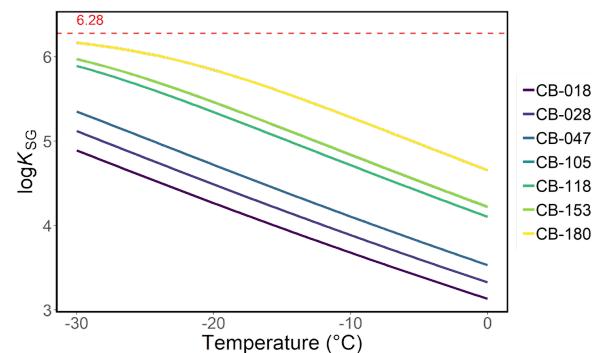


(g) logK<sub>SG</sub> as a function of temperature.

Equilibrium

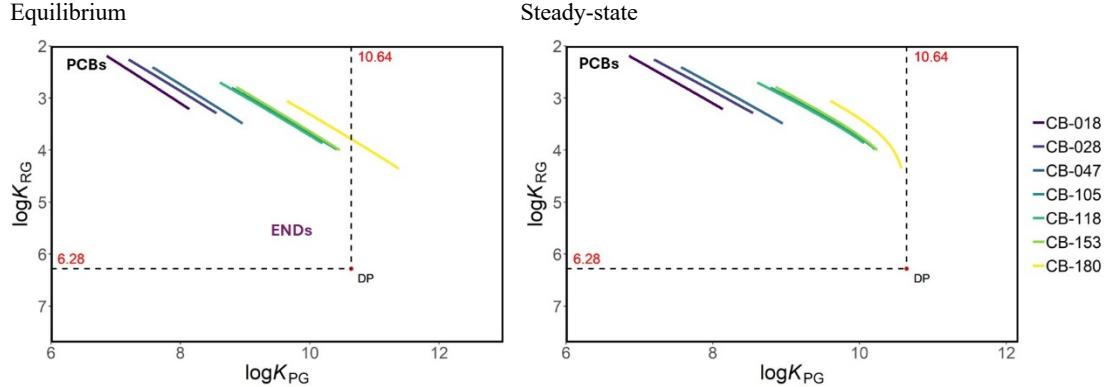


Steady-state

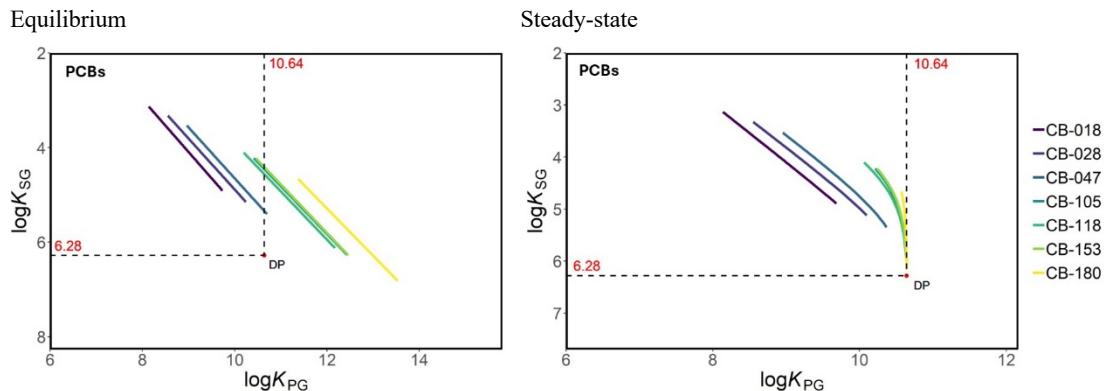


*Step 3 Plot  $\log K_{PG}$  and  $\log K_{RG}$  ( $\log K_{SG}$ ) at the same temperature as x and y axes*

(h)  $\log K_{RG}$  as a function of  $\log K_{PG}$ . CSMs when  $t \geq 0$  °C.



(i)  $\log K_{SG}$  as a function of  $\log K_{PG}$ . CSMs when  $t < 0$  °C.

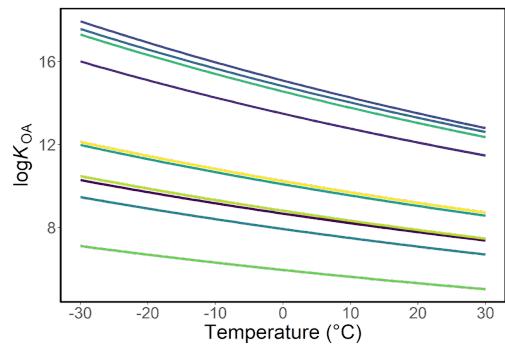


Parameters for 7 selected PCBs.  $\log K_{OA}$  (a),  $\log K_{WA}$  (b),  $\log K_{IA}$  (c), and  $\log K_{JA}$  (d) as functions of temperature.  $\log K_{PG}$  (e),  $\log K_{RG}$  (f), and  $\log K_{SG}$  (g) as functions of temperature.  $\log K_{RG}$  (h) and  $\log K_{RG}$  (i) as functions of  $\log K_{PG}$ . The left panels are from equilibrium equations, and the right panels are from steady-state equations.

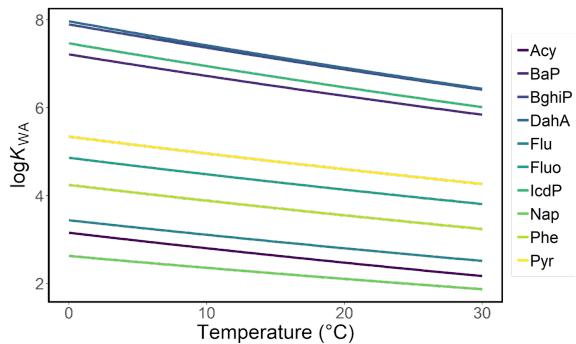
**Figure S4** Steps to place the PAHs in the CSMs

*Step 1 Calculate  $\log K_{OA}$ ,  $\log K_{WA}$ ,  $\log K_{IA}$ , and  $\log K_{JA}$  as functions of temperature*

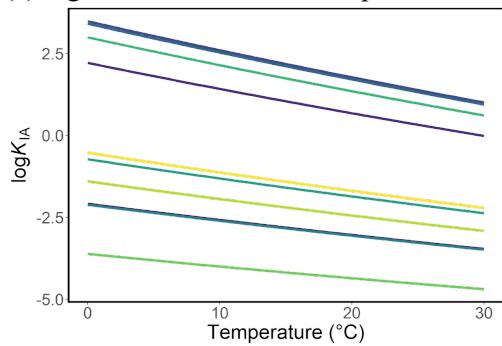
(a)  $\log K_{OA}$  as a function of temperature.



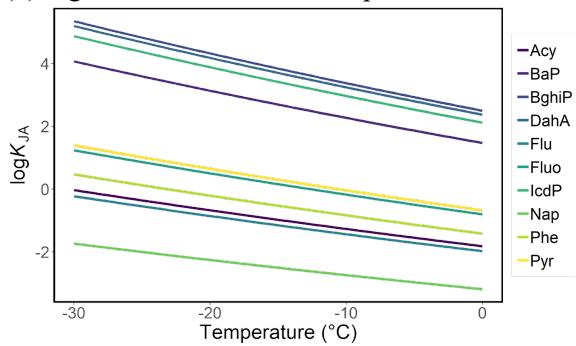
(b)  $\log K_{WA}$  as a function of temperature.



(c)  $\log K_{IA}$  as a function of temperature.



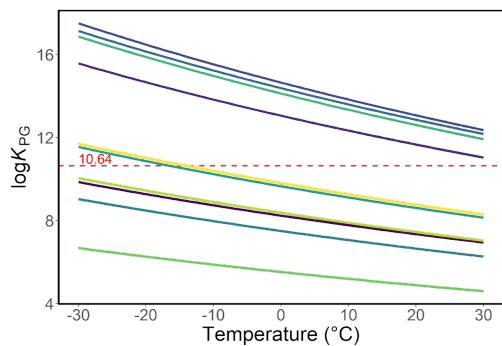
(d)  $\log K_{JA}$  as a function of temperature.



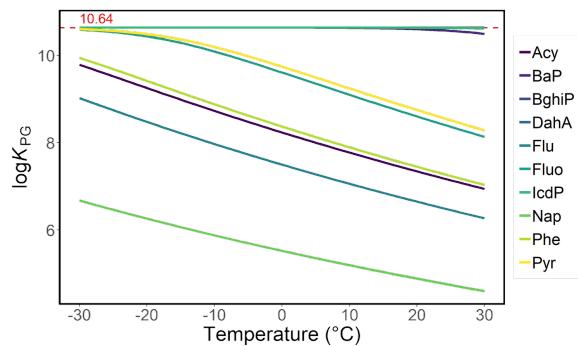
*Step 2 Calculate logK<sub>PG</sub>, logK<sub>RG</sub>, and logK<sub>SG</sub> as functions of temperature*

(e) logK<sub>PG</sub> as a function of temperature.

Equilibrium

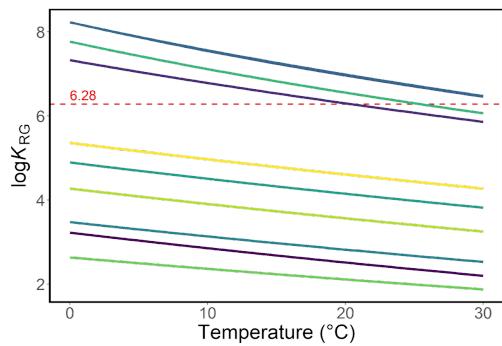


Steady-state

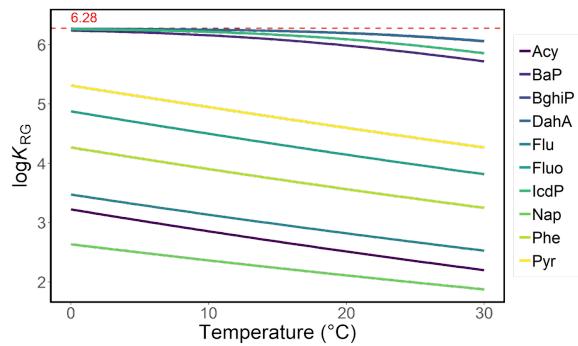


(f) logK<sub>RG</sub> as a function of temperature.

Equilibrium

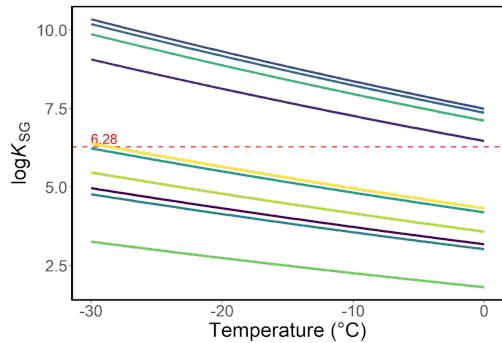


Steady-state

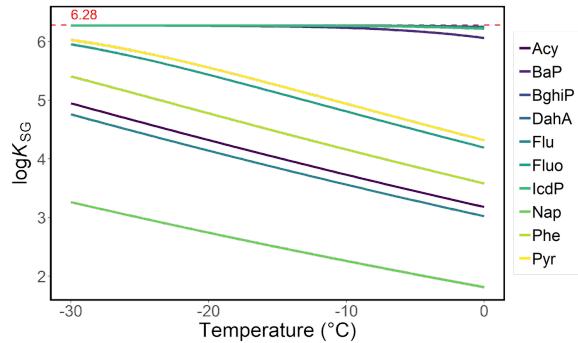


(g) logK<sub>SG</sub> as a function of temperature.

Equilibrium



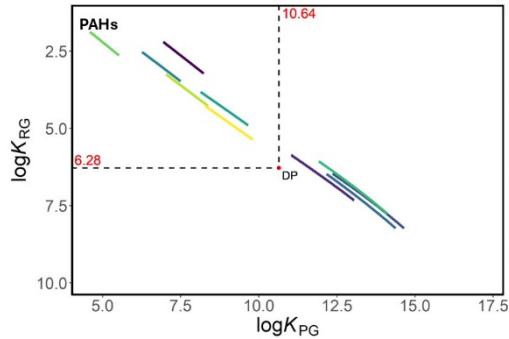
Steady-state



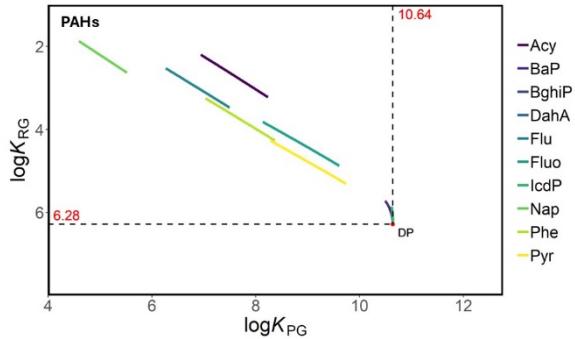
*Step 3 Plot  $\log K_{PG}$  and  $\log K_{RG}$  ( $\log K_{SG}$ ) at the same temperature as x and y axes*

(h)  $\log K_{RG}$  as a function of  $\log K_{PG}$ . CSMs when  $t \geq 0$  °C.

Equilibrium

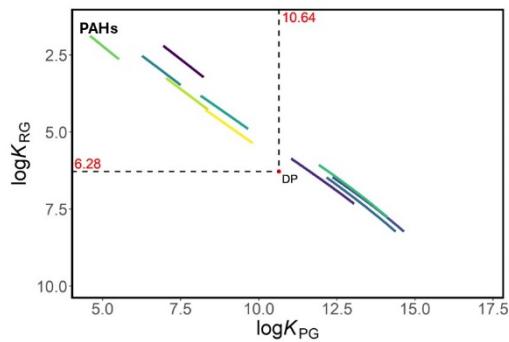


Steady-state

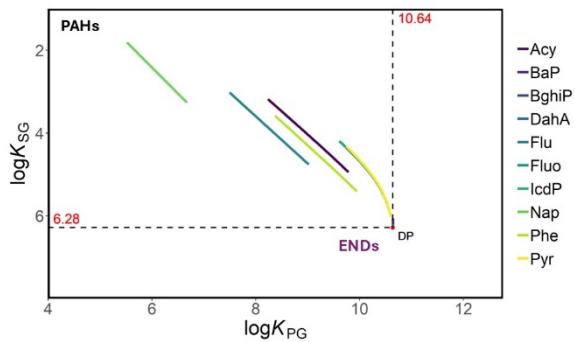


(i)  $\log K_{SG}$  as a function of  $\log K_{PG}$ . CSMs when  $t < 0$  °C.

Equilibrium



Steady-state

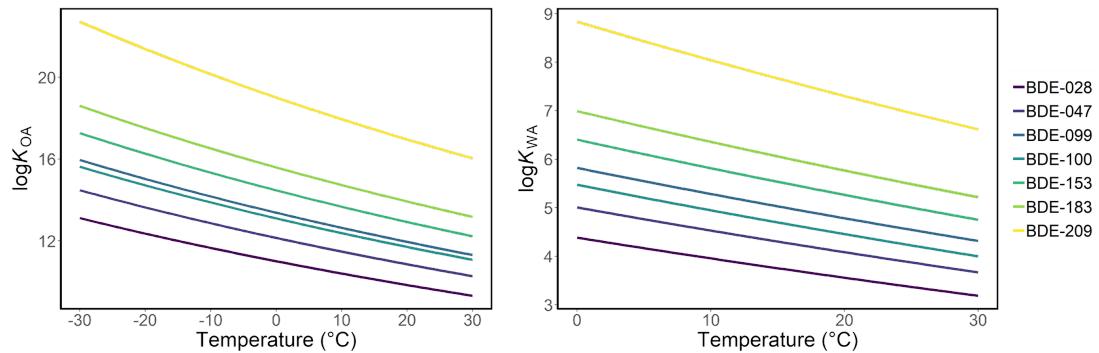


Parameters for 10 selected PAHs.  $\log K_{OA}$  (a),  $\log K_{WA}$  (b),  $\log K_{IA}$  (c), and  $\log K_{JA}$  (d) as functions of temperature.  $\log K_{PG}$  (e),  $\log K_{RG}$  (f), and  $\log K_{SG}$  (g) as functions of temperature.  $\log K_{RG}$  (h) and  $\log K_{RG}$  (i) as functions of  $\log K_{PG}$ . The left panels are from equilibrium equations, and the right panels are from steady-state equations.

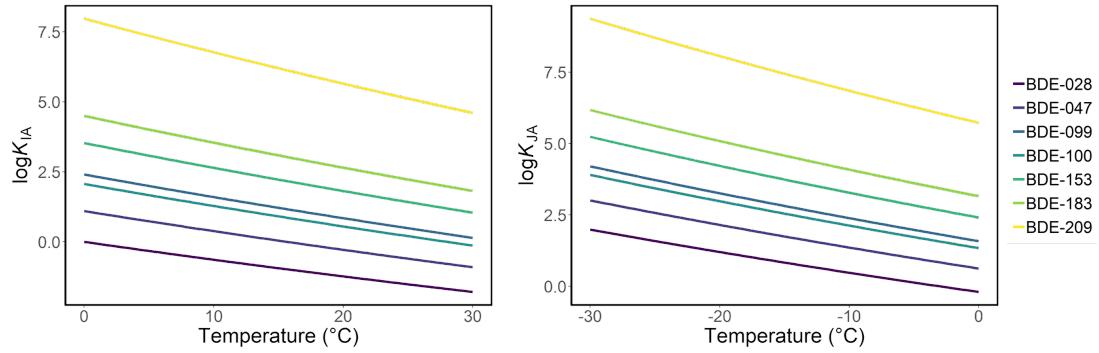
**Figure S5** Steps to place the PBDEs in the CSMs

*Step 1 Calculate log $K_{OA}$ , log $K_{WA}$ , log $K_{IA}$ , and log $K_{JA}$  as functions of temperature*

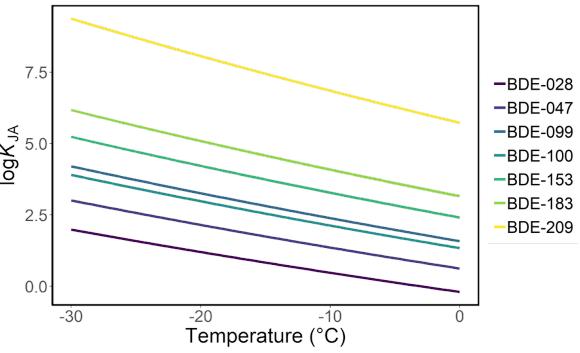
(a) log $K_{OA}$  as a function of temperature. (b) log $K_{WA}$  as a function of temperature.



(c) log $K_{IA}$  as a function of temperature.



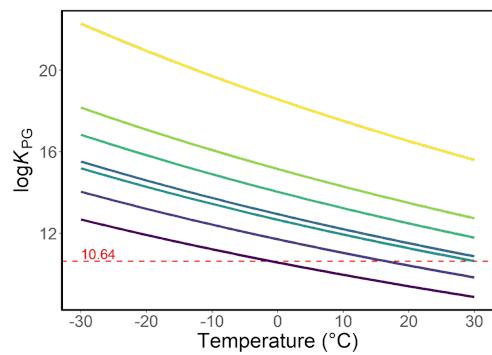
(d) log $K_{JA}$  as a function of temperature.



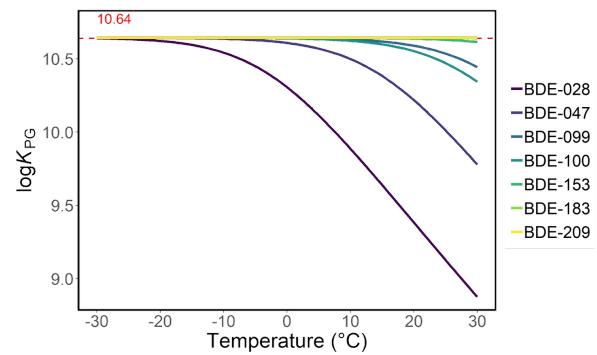
*Step 2 Calculate logK<sub>PG</sub>, logK<sub>RG</sub>, and logK<sub>SG</sub> as functions of temperature*

(e) logK<sub>PG</sub> as a function of temperature.

Equilibrium

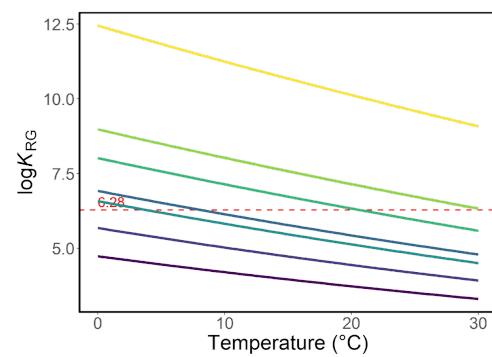


Steady-state

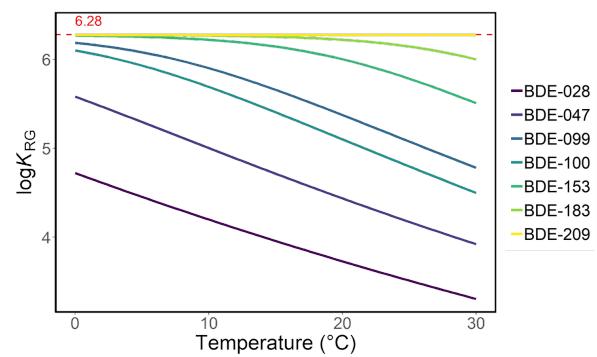


(f) logK<sub>RG</sub> as a function of temperature.

Equilibrium

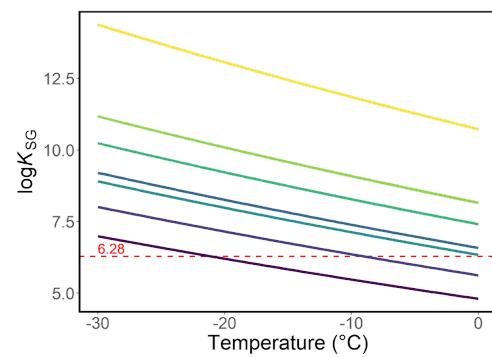


Steady-state

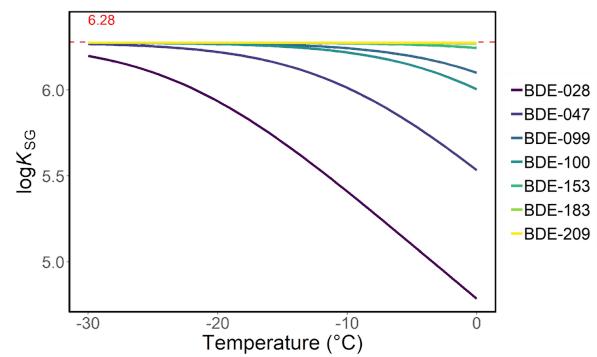


(g) logK<sub>SG</sub> as a function of temperature.

Equilibrium

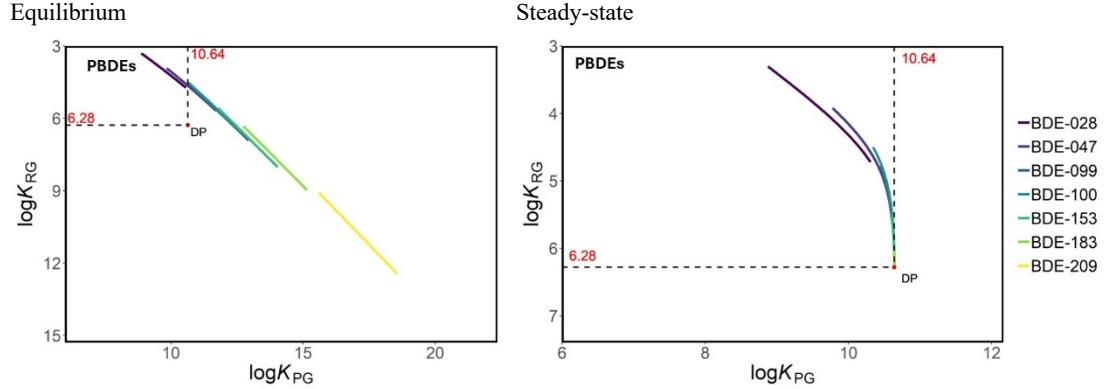


Steady-state

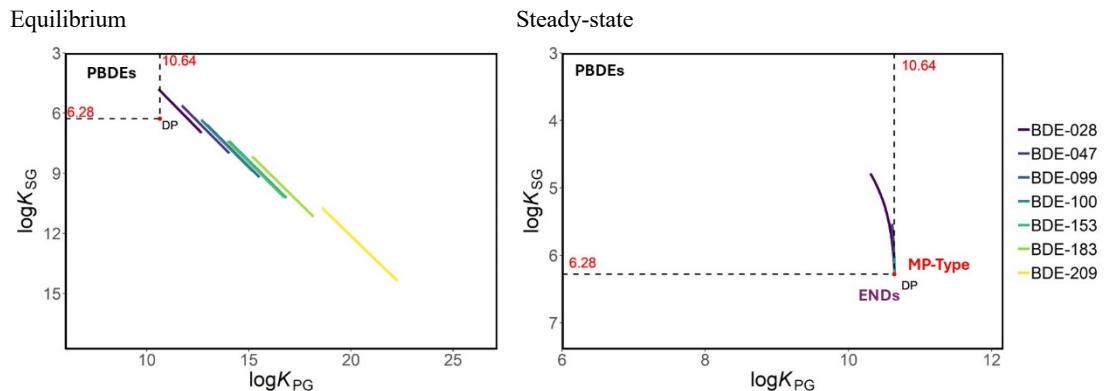


*Step 3 Plot  $\log K_{PG}$  and  $\log K_{RG}$  ( $\log K_{SG}$ ) at the same temperature as x and y axes*

(h)  $\log K_{RG}$  as a function of  $\log K_{PG}$ . CSMs when  $t \geq 0$  °C.

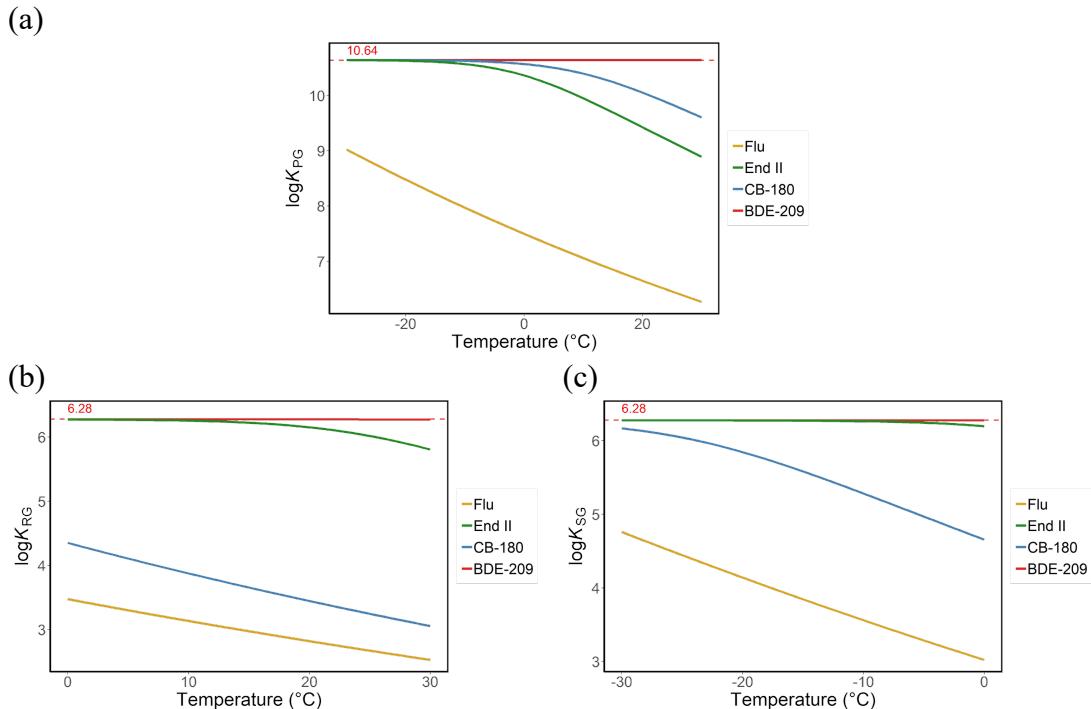


(i)  $\log K_{SG}$  as a function of  $\log K_{PG}$ . CSMs when  $t < 0$  °C.



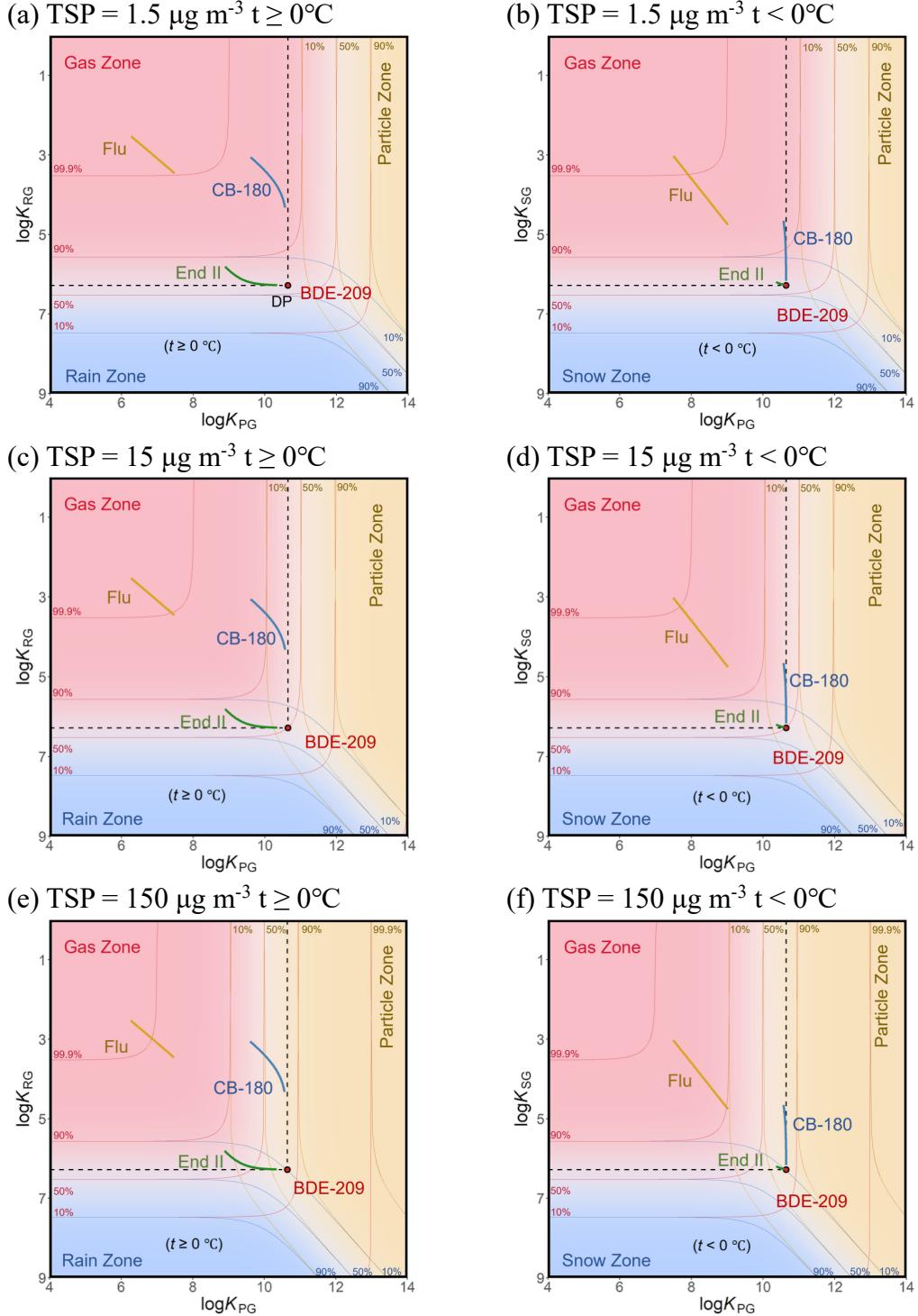
Parameters for 7 selected PBDEs.  $\log K_{OA}$  (a),  $\log K_{WA}$  (b),  $\log K_{IA}$  (c), and  $\log K_{JA}$  (d) as functions of temperature.  $\log K_{PG}$  (e),  $\log K_{RG}$  (f), and  $\log K_{SG}$  (g) as functions of temperature.  $\log K_{RG}$  (h) and  $\log K_{RG}$  (i) as functions of  $\log K_{PG}$ . The left panels are from equilibrium equations, and the right panels are from steady-state equations.

**Figure S6**  $\log K_{\text{PG}}$ ,  $\log K_{\text{RG}}$ , and  $\log K_{\text{SG}}$  for four selected SVOCs as functions of temperature



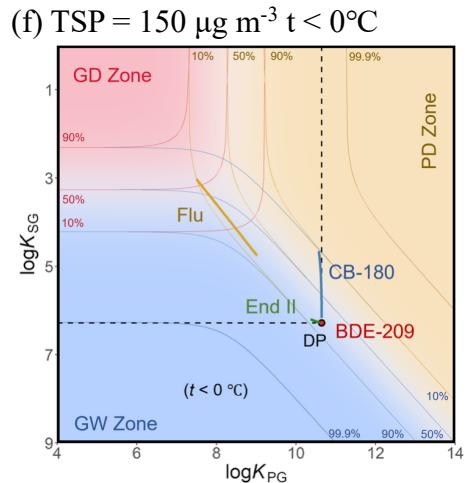
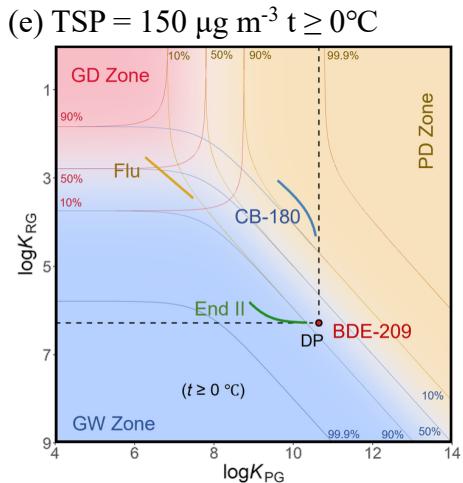
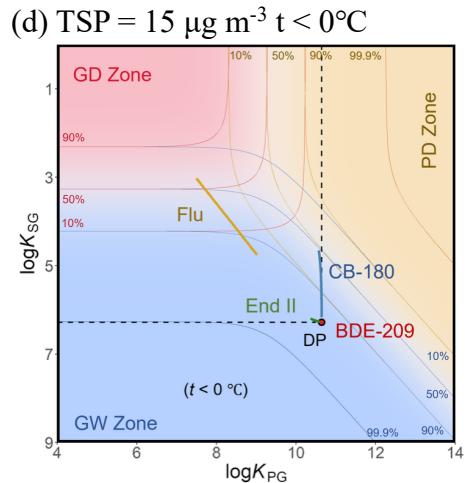
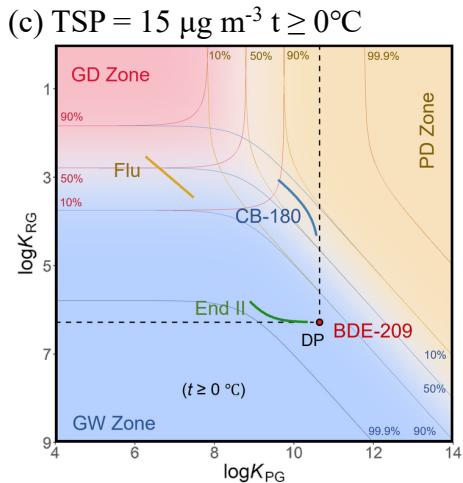
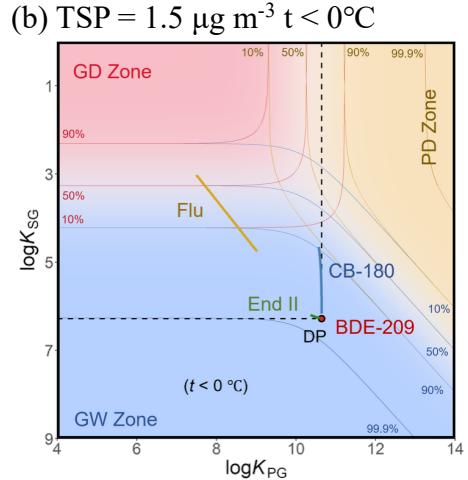
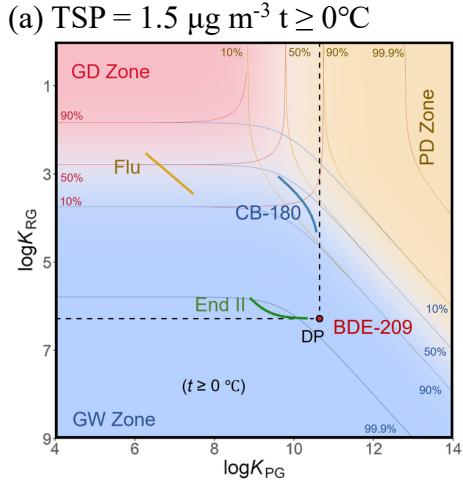
Variation of  $\log K_{\text{PG}}$ ,  $\log K_{\text{RG}}$ , and  $\log K_{\text{SG}}$  for the selected four SVOCs, Flu, End II, CB-180, and BDE-209, as functions of temperature, with the upper limit values of  $\log K_{\text{PG}}$  (a) = 10.64,  $\log K_{\text{RG}}$  (b) and  $\log K_{\text{SG}}$  (c) = 6.28 under steady-state conditions, showing their different characteristics. The EQ-Type SVOCs, such as Flu, are approximately straight lines far away from the upper limits. The PR-Type SVOCs, such as End II, are curves reaching the upper limit lines of  $\log K_{\text{RG}}$  or  $\log K_{\text{SG}}$  with decreasing temperature. The curves of the PA-Type SVOCs, such as CB-180, gradually approach the upper limit of  $\log K_{\text{PG}}$ . The MP-Type SVOCs, such as BDE-209, are coinciding with the upper limits of  $\log K_{\text{PG}}$  and  $\log K_{\text{RG}}$  ( $\log K_{\text{SG}}$ ), independent of temperature.

**Figure S7** Sensitivity analysis of TSP on distribution



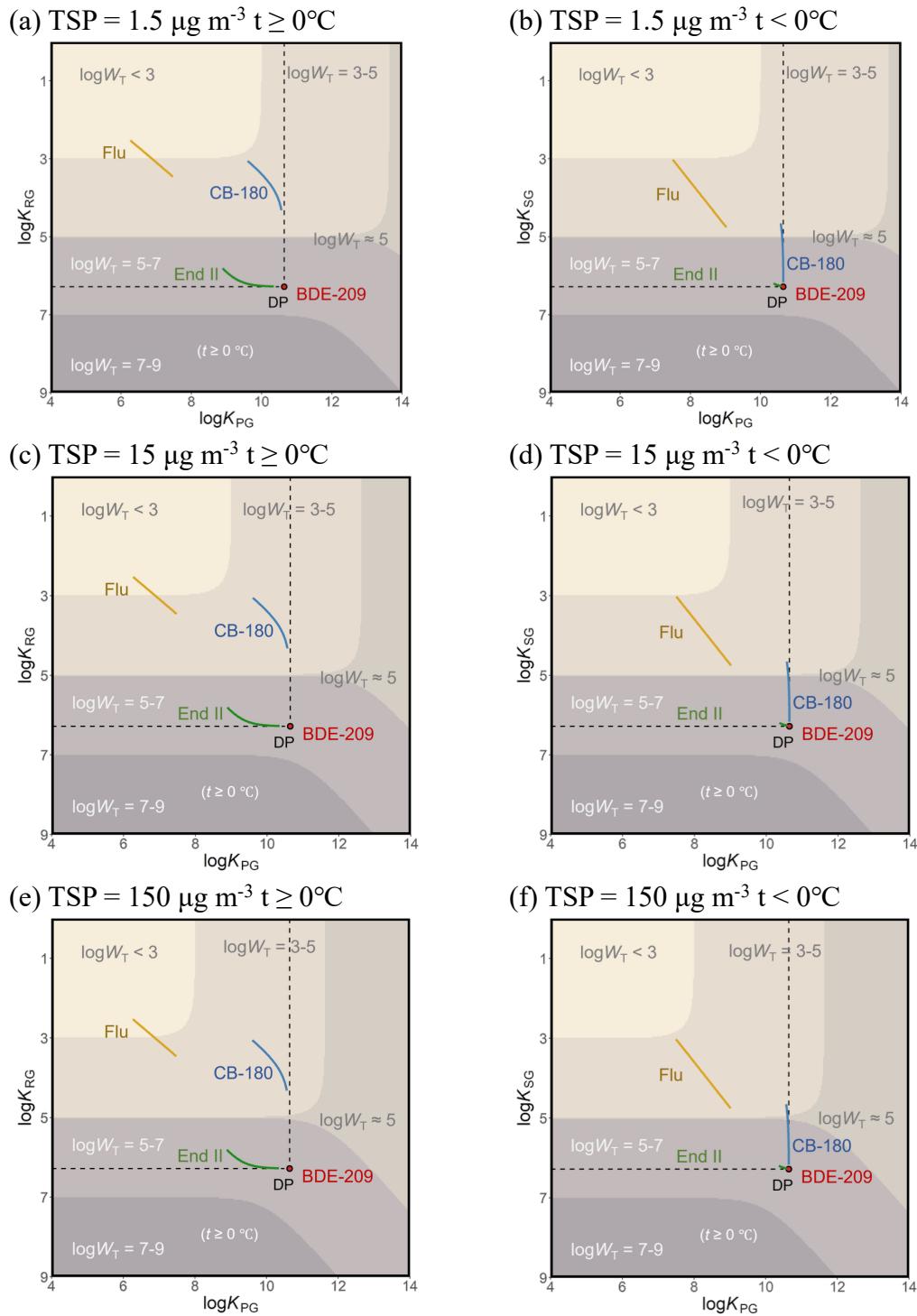
Distribution fraction ( $\Phi$ ) CSMs with different TSP values (a) TSP =  $1.5 \mu\text{g m}^{-3}$  when  $0 \leq t < 30^\circ\text{C}$ ; (b) TSP =  $1.5 \mu\text{g m}^{-3}$  when  $-30 \leq t < 0^\circ\text{C}$ ; (c) TSP =  $15 \mu\text{g m}^{-3}$  when  $0 \leq t < 30^\circ\text{C}$ ; (d) TSP =  $15 \mu\text{g m}^{-3}$  when  $-30 \leq t < 0^\circ\text{C}$ ; (e) TSP =  $150 \mu\text{g m}^{-3}$  when  $0 \leq t < 30^\circ\text{C}$ ; (f) TSP =  $150 \mu\text{g m}^{-3}$  when  $-30 \leq t < 0^\circ\text{C}$ .

**Figure S8** Sensitivity analysis of TSP on deposition



Deposition contribution ( $\Psi$ ) CSMs with different TSP values (a)  $\text{TSP} = 1.5 \mu\text{g m}^{-3}$  when  $0 \leq t < 30^\circ\text{C}$ ; (b)  $\text{TSP} = 1.5 \mu\text{g m}^{-3}$  when  $-30 \leq t < 0^\circ\text{C}$ ; (c)  $\text{TSP} = 15 \mu\text{g m}^{-3}$  when  $0 \leq t < 30^\circ\text{C}$ ; (d)  $\text{TSP} = 15 \mu\text{g m}^{-3}$  when  $-30 \leq t < 0^\circ\text{C}$ ; (e)  $\text{TSP} = 150 \mu\text{g m}^{-3}$  when  $0 \leq t < 30^\circ\text{C}$ ; (f)  $\text{TSP} = 150 \mu\text{g m}^{-3}$  when  $-30 \leq t < 0^\circ\text{C}$ .

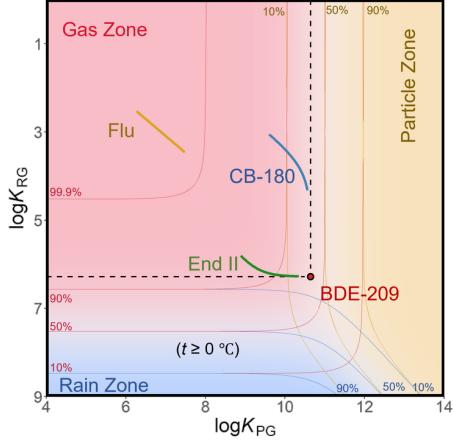
**Figure S9** Sensitivity analysis of TSP on scavenging



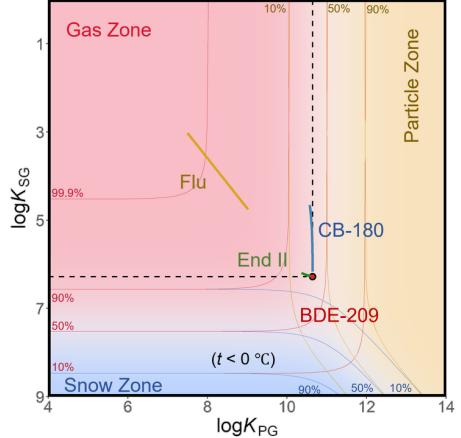
Scavenging ratio( $W$ ) CSMs with different TSP values (a) TSP = 1.5  $\mu\text{g m}^{-3}$  when  $0 \leq t < 30^\circ\text{C}$ ; (b) TSP = 1.5  $\mu\text{g m}^{-3}$  when  $-30 \leq t < 0^\circ\text{C}$ ; (c) TSP = 15  $\mu\text{g m}^{-3}$  when  $0 \leq t < 30^\circ\text{C}$ ; (d) TSP = 15  $\mu\text{g m}^{-3}$  when  $-30 \leq t < 0^\circ\text{C}$ ; (e) TSP = 150  $\mu\text{g m}^{-3}$  when  $0 \leq t < 30^\circ\text{C}$ ; (f) TSP = 150  $\mu\text{g m}^{-3}$  when  $-30 \leq t < 0^\circ\text{C}$ .

**Figure S10** Sensitivity analysis of precipitation rate on distribution

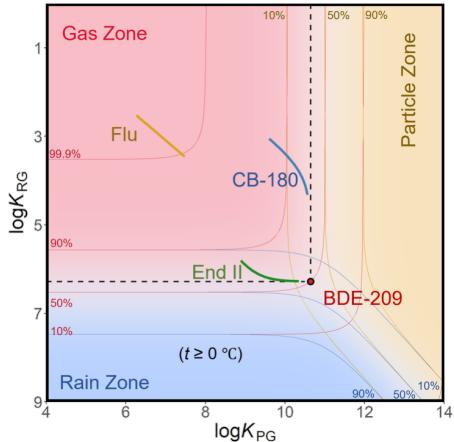
(a)  $U_R = 3.2 \times 10^{-4} \text{ m h}^{-1} t \geq 0^\circ\text{C}$



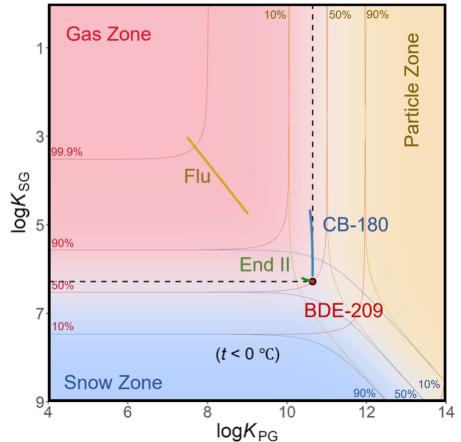
(b)  $U_S = 1.1 \times 10^{-4} \text{ m h}^{-1} t < 0^\circ\text{C}$



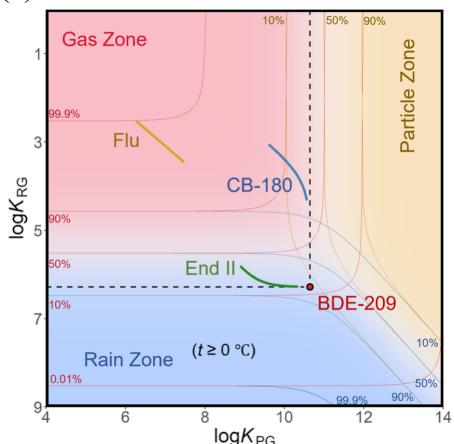
(c)  $U_R = 3.2 \times 10^{-3} \text{ m h}^{-1} t \geq 0^\circ\text{C}$



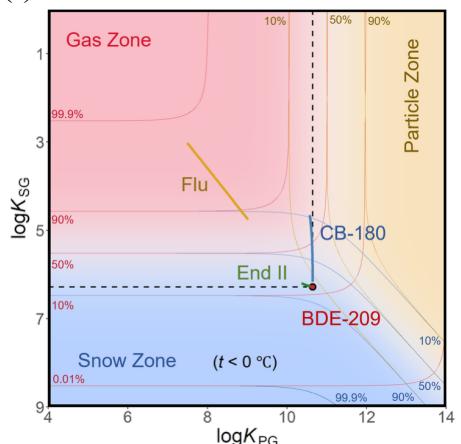
(d)  $U_S = 1.1 \times 10^{-3} \text{ m h}^{-1} t < 0^\circ\text{C}$



(e)  $U_R = 3.2 \times 10^{-2} \text{ m h}^{-1} t \geq 0^\circ\text{C}$

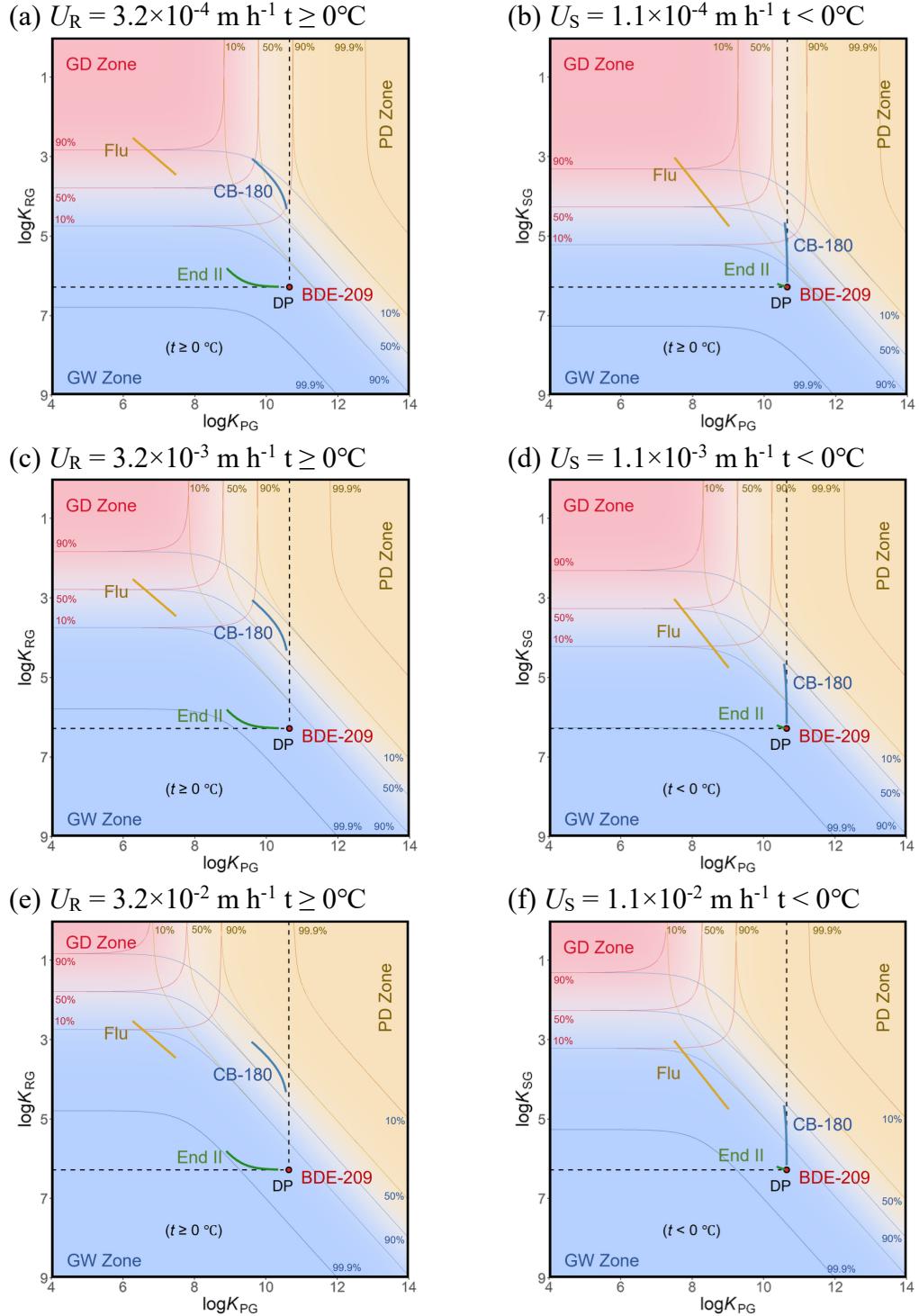


(f)  $U_S = 1.1 \times 10^{-2} \text{ m h}^{-1} t < 0^\circ\text{C}$



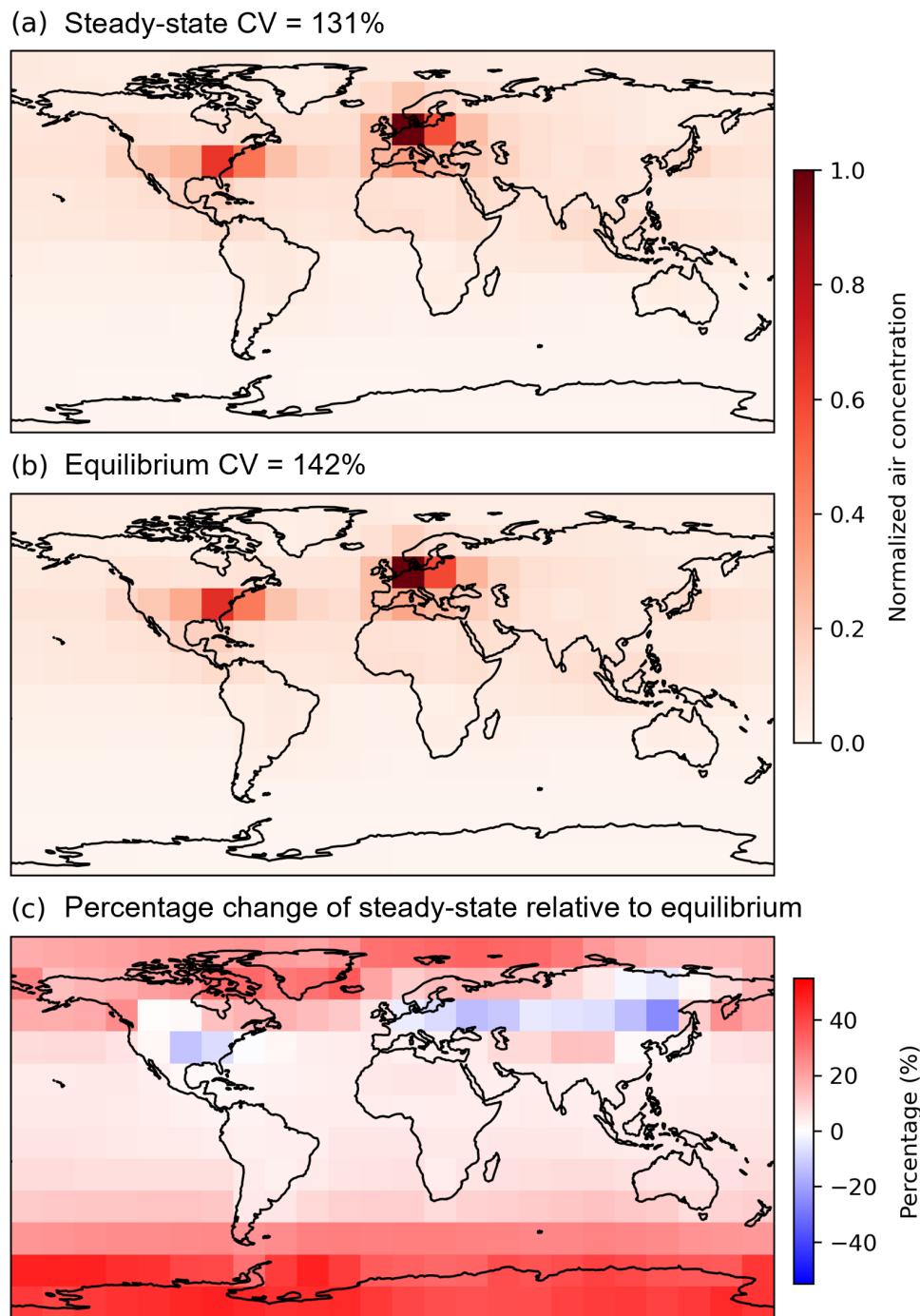
Distribution fraction( $\Phi$ ) CSMs with different precipitation values (a)  $U_R = 3.2 \times 10^{-4} \text{ m h}^{-1}$  ( $V_W = 3 \times 10^{-8}$ ) when  $0 \leq t < 30^\circ\text{C}$ ; (b)  $U_S = 1.1 \times 10^{-4} \text{ m h}^{-1}$  ( $V_W = 3 \times 10^{-8}$ ) when  $-30 \leq t < 0^\circ\text{C}$ ; (c)  $U_R = 3.2 \times 10^{-3} \text{ m h}^{-1}$  ( $V_W = 3 \times 10^{-7}$ ) when  $0 \leq t < 30^\circ\text{C}$ ; (d)  $U_S = 1.1 \times 10^{-3} \text{ m h}^{-1}$  ( $V_W = 3 \times 10^{-7}$ ) when  $-30 \leq t < 0^\circ\text{C}$ ; (e)  $U_R = 3.2 \times 10^{-2} \text{ m h}^{-1}$  ( $V_W = 3 \times 10^{-6}$ ) when  $0 \leq t < 30^\circ\text{C}$ ; (f)  $U_S = 1.1 \times 10^{-2} \text{ m h}^{-1}$  ( $V_W = 3 \times 10^{-6}$ ) when  $-30 \leq t < 0^\circ\text{C}$ .

**Figure S11** Sensitivity analysis of precipitation rate on deposition



Deposition contribution( $\Psi$ ) CSMs with different precipitation values (a)  $U_R = 3.2 \times 10^{-4} \text{ m h}^{-1}$  ( $V_W = 3 \times 10^{-8}$ ) when  $0 \leq t < 30^\circ\text{C}$ ; (b)  $U_S = 1.1 \times 10^{-4} \text{ m h}^{-1}$  ( $V_W = 3 \times 10^{-8}$ ) when  $-30 \leq t < 0^\circ\text{C}$ ; (c)  $U_R = 3.2 \times 10^{-3} \text{ m h}^{-1}$  ( $V_W = 3 \times 10^{-7}$ ) when  $0 \leq t < 30^\circ\text{C}$ ; (d)  $U_S = 1.1 \times 10^{-3} \text{ m h}^{-1}$  ( $V_W = 3 \times 10^{-7}$ ) when  $-30 \leq t < 0^\circ\text{C}$ ; (e)  $U_R = 3.2 \times 10^{-2} \text{ m h}^{-1}$  ( $V_W = 3 \times 10^{-6}$ ) when  $0 \leq t < 30^\circ\text{C}$ ; (f)  $U_S = 1.1 \times 10^{-2} \text{ m h}^{-1}$  ( $V_W = 3 \times 10^{-6}$ ) when  $-30 \leq t < 0^\circ\text{C}$ .

**Figure S12** Result of BETR-Global: normalized global air concentration of CB-180



Result of BETR-Global: normalized global air concentration of CB-180 under steady state (a), equilibrium (b), and percentage change of steady-state relative to equilibrium(c)

## Tables

**Table S1** Nomenclature and default values

Symbol	Value	Unit	Meaning
$A$	-	-	Antoine parameter, the intercept
$A_0$	1 <sup>a</sup>	$\text{m}^2$	Area of air-surface interface
$A_{\text{GR}}$	-	$\text{m}^2$	Area of gas-raindrop interface
$A_{\text{GS}}$	-	$\text{m}^2$	Area of gas-snowflake interface
$\alpha_{\text{P}}$	-	-	Non-equilibrium term of $K_{\text{PG}}$
$\alpha_{\text{R}}$	-	-	Non-equilibrium term of $K_{\text{RG}}$
$\alpha_{\text{S}}$	-	-	Non-equilibrium term of $K_{\text{SG}}$
$B$	-	-	Antoine parameter, the slope
$C_{\text{G}}$	-	$\text{mol m}^{-3}$	Gas concentration
$C_{\text{G};\text{E}}$	-	$\text{mol m}^{-3}$	Gas concentration under equilibrium with other media
$C_{\text{G};\text{S}}$	-	$\text{mol m}^{-3}$	Gas concentration under steady-state with other media
$C_{\text{P}}$	-	$\text{mol m}^{-3}$	Particle concentration, divided by volume of particle
$C_{\text{P};\text{E}}$	-	$\text{mol m}^{-3}$	Particle concentration under equilibrium with other media, divided by volume of particle
$C_{\text{P};\text{S}}$	-	$\text{mol m}^{-3}$	Particle concentration under steady-state with other media, divided by volume of particle
$C'_{\text{P};\text{E}}$	-	$\text{mol m}^{-3}$	Particle concentration under equilibrium, divided by volume of air
$C_{\text{R}}$	-	$\text{mol m}^{-3}$	Raindrop concentration, divided by volume of rain
$C_{\text{R};\text{E}}$	-	$\text{mol m}^{-3}$	Raindrop concentration under equilibrium, divided by volume of rain
$C_{\text{R};\text{S}}$	-	$\text{mol m}^{-3}$	Raindrop concentration under steady-state, divided by volume of rain
$C_{\text{S}}$	-	$\text{mol m}^{-3}$	Snowflake concentration, divided by volume of water equivalent snowflake
$C_{\text{S};\text{E}}$	-	$\text{mol m}^{-3}$	Snowflake concentration under equilibrium, divided by volume of water equivalent snowflake
$\text{CTD}$	-	km	Characteristic travel distance
$D_{\text{g}}$	$6.9 \times 10^{-6}$ <sup>b</sup>	$\text{m}^2/\text{s}$	Molecular diffusivities in air
$D_{\text{GDD}}$	-	$\text{mol Pa}^{-1} \text{h}^{-1}$	$D$ value for gas dry deposition
$D_{\text{GR}}$	-	$\text{mol Pa}^{-1} \text{h}^{-1}$	$D$ value for transfer from gas to raindrop
$D_{\text{GRD}}$	-	$\text{mol Pa}^{-1} \text{h}^{-1}$	$D$ value for gas rainfall deposition

<sup>a</sup> The air-surface area is set to 1  $\text{m}^2$  in this study. In fact, it can be set to any value since it is eliminated during the calculation

<sup>b</sup> This value refers to a published paper (Simcik, 2004)<sup>1</sup>

$D_{GS}$	-	$\text{mol Pa}^{-1} \text{ h}^{-1}$	$D$ value for transferal from gas to snowflake
$D_{GSD}$	-	$\text{mol Pa}^{-1} \text{ h}^{-1}$	$D$ value for gas snowfall deposition
$D_{GWD}$	-	$\text{mol Pa}^{-1} \text{ h}^{-1}$	$D$ value for gas wet deposition
$D_{RG}$	-	$\text{mol Pa}^{-1} \text{ h}^{-1}$	$D$ value for transferal from raindrop to gas
$D_{SG}$	-	$\text{mol Pa}^{-1} \text{ h}^{-1}$	$D$ value for transferal from snowflake to gas
$f_G$	-	Pa	Fugacity of gas
$f_{OM}$	0.2 <sup>c</sup>	-	Fraction of organic matter in particle
$f_P$	-	Pa	Fugacity of particle
$f_R$	-	Pa	Fugacity of raindrop
$f_S$	-	Pa	Fugacity of snowflake
$h$	1000 <sup>c</sup>	m	Height of the partitioning start
$k_{GD}$	2 <sup>c</sup>	$\text{m h}^{-1}$	Gaseous dry deposition rate
$k_{GR}$	681 <sup>d</sup>	$\text{m h}^{-1}$	Air side air-raindrop mass transfer coefficient
$k_{GS}$	104 <sup>e</sup>	$\text{m h}^{-1}$	Air side air-snowflake mass transfer coefficient
$k_{PD}$	1 <sup>d</sup>	$\text{m h}^{-1}$	Particulate dry deposition rate
$K_{IA}$	-	m	Water surface-air adsorption coefficient
$K_{OA}$	-	-	Octanol-air partition ratio
$K_{PE}$	-	$\text{m}^3 \mu\text{g}^{-1}$	Particle-gas partition coefficient under equilibrium condition
$K_{PG}$	-	-	Dimensionless particle-gas partition ratio
$K_{RG}$	-	-	Dimensionless rain-gas partition ratio
$K_{JA}$	-	m	Snow surface-air adsorption coefficient
$K_{SG}$	-	-	Dimensionless snow-gas partition ratio
$K_{WA}$	-	-	Water-air partition ratio
$N_{G-R}$	-	$\text{mol h}^{-1}$	Flux of SVOCs from gas phase to rain phase
$N_{R-G}$	-	$\text{mol h}^{-1}$	Flux of SVOCs from rain phase to gas phase
$N_{R-D}$	-	$\text{mol h}^{-1}$	Flux of rain-bound SVOCs from air to earth surface
$N_{G-S}$	-	$\text{mol h}^{-1}$	Flux of SVOCs from gas phase to snow phase
$N_{S-G}$	-	$\text{mol h}^{-1}$	Flux of SVOCs from snow phase to gas phase
$N_{S-D}$	-	$\text{mol h}^{-1}$	Flux of snow-bound SVOCs from air to earth surface
$r_R$	$1 \times 10^{-4}$ <sup>f</sup>	m	Average radius of raindrop (including drizzle)

<sup>c</sup> This value refers to a published paper (Lei and Wania, 2004)<sup>2</sup>

<sup>d</sup> Please see Eq. S13

<sup>e</sup> Please see Eq. S16

<sup>f</sup> Lei and Wania<sup>2</sup> set the raindrop radius to 1 mm. But considering drizzle,<sup>3</sup> which has smaller diameter, hardly deposit, but can sorb gaseous SVOCs as well, we set a relatively small radius as the average radius of drops in the atmosphere and set a relatively small velocity as the average raindrop falling velocity. However,

$r_s$	$2 \times 10^{-3}$ g	m	Average dynamic radius of snow (including graupel and wet snow)
$\rho_p$	1500 <sup>c</sup>	kg m <sup>-3</sup>	Density of particle
$\rho_w$	1000	kg m <sup>-3</sup>	Density of water
$S$	-	-	Sensitivity
$SAs$	100 <sup>d</sup>	m <sup>2</sup> kg <sup>-1</sup>	Specific area of snowflake
$TH_1$	-	-	Temperature threshold 1
$TH_2$	-	-	Temperature threshold 2
$T/t$	-	K	Temperature
TSP	15 <sup>g</sup>	$\mu\text{g m}^{-3}$	Total suspended particles in a precipitation weather
$U_w$	-	m h <sup>-1</sup>	Instantaneous precipitation rate, including $U_R$ and $U_S$
$U_R$	$3.2 \times 10^{-3}$ <sup>h</sup>	m h <sup>-1</sup>	Instantaneous rain rate
$U_S$	$1.1 \times 10^{-3}$ <sup>i</sup>	m h <sup>-1</sup>	Instantaneous snow rate
$v_a$	$1.48 \times 10^{-5}$	m <sup>2</sup> s <sup>-1</sup>	Kinematic viscosity of air
$v_p$	$10^{-11}$ <sup>i</sup>	-	Volume fraction of particle in air
$v_w$	$3 \times 10^{-7}$ <sup>d</sup>	-	Volume fraction of water equivalent precipitation in air
$v_r$	$3 \times 10^{-7}$	-	Volume fraction of rain water in air
$v_s$	$3 \times 10^{-7}$	-	Volume fraction of water equivalent snow in air
$u_R$	3 <sup>i</sup>	m s <sup>-1</sup>	Average raindrop terminal velocity
$u_S$	1 <sup>i</sup>	m s <sup>-1</sup>	Average snowflake terminal velocity
$W_G$	-	-	Gas scavenging ratio
$W_P$	$10^5$ <sup>d</sup>	-	Particle scavenging ratio
$W_T$	-	-	Total rain/snow scavenging ratio
$Z_G$	-	mol m <sup>-3</sup> Pa <sup>-1</sup>	Fugacity capacity of gas
$Z_P$	-	mol m <sup>-3</sup> Pa <sup>-1</sup>	Fugacity capacity of particle
$Z_R$	-	mol m <sup>-3</sup> Pa <sup>-1</sup>	Fugacity capacity of raindrop
$Z_s$	-	mol m <sup>-3</sup> Pa <sup>-1</sup>	Fugacity capacity of snow
$\Psi$	-	-	Chemicals' deposition contribution
$\Phi$	-	-	Chemicals' phase distribution fraction in the atmosphere

<sup>a</sup> considering graupel and snow clumps, we assume a relatively medium size for snow.<sup>3</sup>

<sup>b</sup> This is a reasonable assumption of total suspended particle value during precipitation.

<sup>c</sup> See [Text S2](#)

**Table S2** Physical–chemical properties and measurements for 36 selected chemicals

Chemicals (36)	Abbr.	<i>A</i> <sub>AW</sub>	<i>B</i> <sub>AW</sub>	<i>A</i> <sub>OA</sub>	<i>B</i> <sub>OA</sub>	<i>A</i> <sub>IA</sub>	<i>B</i> <sub>IA</sub>	<i>A</i> <sub>JA</sub>	<i>B</i> <sub>JA</sub>	Sample number		
										<i>logK</i> <sub>PG</sub>	<i>logK</i> <sub>RG</sub>	<i>logK</i> <sub>SG</sub>
<b>OCPs (12)</b>												
alpha-Hexachlorocyclohexane	α-HCH	9.09	-3863	-5.64	3913	-18.93	5397	-17.90	4828	10 (911)	10 (32)	10 (30)
beta-Hexachlorocyclohexane	β-HCH	8.67	-3825	-5.54	3945	-18.94	5403	-17.94	4851	10 (1024)	10 (16)	10 (18)
gamma-Hexachlorocyclohexane	γ-HCH	8.58	-3799	-5.46	3918	-18.86	5362	-17.90	4825	10 (1343)	10 (21)	10 (23)
o,p'-DDT	o,p'-DDT	8.74	-3523	-5.37	4468	-17.89	4830	-17.78	4763	10 (329)	10 (12)	8 (8)
o,p'-DDD	o,p'-DDD	8.24	-3610	-5.97	4760	-18.35	5085	-18.16	4968	10 (304)	0 (0)	0 (0)
o,p'-DDE	o,p'-DDE	8.21	-3174	-5.16	4183	-17.03	4362	-17.16	4426	10 (308)	0 (0)	0 (0)
p,p'-DDT	p,p'-DDT	8.25	-3350	-5.58	4642	-17.70	4730	-17.78	4760	10 (1257)	10 (22)	10 (17)
p,p'-DDD	p,p'-DDD	7.92	-3401	-5.73	4672	-18.01	4899	-17.94	4849	10 (305)	0 (0)	0 (0)
p,p'-DDE	p,p'-DDE	8.26	-3252	-6.29	4780	-17.63	4687	-17.74	4738	10 (336)	10 (34)	10 (29)
Endosulfan I	End I	11.59	-5006	-6.99	4970	-21.77	6949	-19.93	5939	10 (1456)	10 (22)	10 (23)
Endosulfan II	End II	11.87	-5176	-6.93	4930	-22.11	7136	-20.09	6026	10 (833)	10 (13)	10 (14)
Endosulfan sulfate	End sul	10.89	-5683	-7.32	5588	-24.12	8234	-21.55	6821	10 (582)	8 (8)	10 (14)
<b>PCBs (7)</b>												
2,2',5-Trichlorobiphenyl	CB-18	6.83	-2726	-4.36	3532	-15.96	3778	-16.27	3934	10 (428)	10 (13)	9 (9)
2,4,4'-Trichlorobiphenyl	CB-28	6.72	-2712	-4.72	3744	-16.15	3879	-16.46	4039	10 (453)	10 (15)	9 (9)
2,2',4,4'-Tetrachlorobiphenyl	CB-47	7.00	-2841	-4.70	3850	-16.38	4004	-16.65	4147	10 (428)	10 (10)	8 (8)
2,3,3',4,4'-Pentachlorobiphenyl	CB-105	7.01	-2957	-5.55	4479	-17.12	4409	-17.36	4530	10 (415)	0 (0)	0 (0)
2,3',4,4',5-Pentachlorobiphenyl	CB-118	7.06	-2942	-5.40	4378	-16.98	4332	-17.24	4465	10 (453)	10 (16)	9 (9)
2,2',4,4',5,5'-Hexachlorobiphenyl	CB-153	7.37	-3061	-5.28	4418	-17.11	4406	-17.35	4528	10 (444)	0 (0)	0 (0)
2,2',3,4,4',5,5'-Heptachlorobiphenyl	CB-180	7.52	-3182	-5.68	4777	-17.59	4665	-17.79	4768	10 (440)	10 (14)	7 (7)
<b>PAHs (10)</b>												
Pyrene	Pyr	5.53	-2970	-5.11	4192	-17.57	4655	-17.46	4584	10 (3644)	10 (33)	10 (30)

Phenanthrene	Phe	5.90	-2771	-4.75	3703	-16.69	4176	-16.71	4177	10 (4159)	10 (35)	10 (31)
Naphthalene	Nap	5.02	-2089	-3.40	2555	-14.48	2967	-14.95	3213	10 (97)	0 (0)	0 (0)
Fluorene	Flu	5.91	-2554	-4.52	3401	-15.97	3784	-16.16	3874	10 (3085)	10 (34)	10 (31)
Fluoranthene	Fluo	5.78	-2907	-5.25	4189	-17.36	4543	-17.33	4514	10 (4240)	10 (33)	10 (33)
Acenaphthylene	Acy	6.81	-2722	-4.44	3581	-16.00	3800	-16.31	3958	10 (436)	0 (0)	0 (0)
Benzo[a]pyrene	BaP	6.66	-3790	-6.92	5574	-20.31	6152	-19.59	5752	10 (1375)	10 (13)	10 (11)
Benzo[ghi]perylene	BghiP	7.13	-4105	-8.08	6327	-21.58	6846	-20.61	6311	10 (1164)	8 (8)	10 (10)
Dibenz[ah]anthracene	DahA	7.55	-4239	-7.54	6106	-21.50	6803	-20.50	6247	10 (354)	3 (3)	0 (0)
Indeno[1,2,3-cd]pyrene	IcdP	7.21	-4009	-7.71	6082	-21.09	6578	-20.24	6106	10 (981)	7 (7)	8 (8)
<b>PBDEs (7)</b>												
2,4,4'-Tribromodiphenyl ether	BDE-28	7.73	-3309	-6.08	4667	-18.09	4941	-17.92	4840	10 (104)	4 (4)	0 (0)
2,2',4,4'-Tetrabromodiphenyl ether	BDE-47	8.52	-3695	-6.75	5161	-19.18	5539	-18.74	5288	10 (228)	6 (6)	0 (0)
2,2',4,4',5-Pentabromodiphenyl ether	BDE-99	9.39	-4155	-7.52	5708	-20.50	6257	-19.70	5812	10 (229)	6 (6)	0 (0)
2,2',4,4',6-Pentabromodiphenyl ether	BDE-100	9.43	-4071	-7.35	5586	-20.17	6074	-19.47	5683	10 (200)	6 (6)	0 (0)
2,2',4,4',5,5'-Hexabromodiphenyl ether	BDE-153	10.30	-4563	-8.22	6198	-21.62	6870	-20.53	6265	10 (186)	6 (6)	0 (0)
2,2',3,4,4',5',6-Heptabromodiphenyl ether	BDE-183	10.95	-4901	-8.81	6665	-22.60	7402	-21.28	6675	10 (92)	2 (2)	0 (0)
Decabromodiphenyl ether	BDE-209	13.61	-6131	-11.03	8205	-26.06	9296	-23.85	8079	10 (750)	10 (11)	7 (0)
Total										360 (14189)	246 (455)	205 (379)

\* Physical-chemical properties for the 36 selected chemicals and the number of samples.  $A$  and  $B$  values are summarized from a previous publication.<sup>4</sup> In the study, we

1) collected pp-LFER parameters for 943 chemicals from the UFZ-LSER database.

2) calculated  $\log K_{XY0}$  (basic partition ratio and adsorption coefficients at a specific temperature  $T_0$ ) and  $\Delta U_{XY}$  (molar internal energy changes between phase X and Y) us the pp-LFER parameters.

3) calculated  $A_{XX}$  and  $B_{XY}$  following the Van't Hoff Equation with  $\log K_{XY0}$  and  $\Delta U_{XY}$  as  $B_{XY} = \Delta U_{XY}/\ln(10)R$  and  $A_{XY} = \log K_{XY0} B_{XY}/T_0$ .

\* The sample number are the number of partition ratios collected and calculated from measurements. The numbers in brackets are the number of records in the dataset and the numbers out brackets are number of random extractions. All the measurements are SVOCs' gas and particle concentration measured by active sampler as well as rain and snow concentration by precipitation sampler. Most of the measurements are collected and calculated from EBAS database (<https://ebas.nilu.no>) and IADN database (<https://iadnviz.iu.edu/about/index.html>)<sup>5</sup>. Data from SAMP II program and some published papers are used as supplement.<sup>6-24</sup> Temperature ( $T$ ) and Total suspended particles concentrations (TSP) used for partition ratios calculation ([Text S1](#)) are downloaded from Copernicus data store (<https://cds.climate.copernicus.eu/>), where TSP is assumed as  $2 \times \text{PM}_{10}$ .

**Table S3** The type categories of the 36 chemicals for the temperature above and below the freezing point

	EQ $t \geq 0$	PA $t < 0$	PR $t \geq 0$	MP $t < 0$
<b>OCPs</b>				
$\alpha$ -HCH	✓			✓
$\beta$ -HCH	✓			✓
$\gamma$ -HCH	✓			✓
o,p'-DDT		✓	✓	
o,p'-DDD		✓	✓	
o,p'-DDE	✓		✓	
p,p'-DDT		✓	✓	
p,p'-DDD		✓	✓	
p,p'-DDE		✓	✓	
End I			✓	✓
End II			✓	✓
End Sul			✓	✓
<b>PCBs</b>				
CB 18	✓	✓		
CB 28	✓	✓		
CB 47	✓	✓		
CB 105	✓		✓	
CB 118	✓		✓	
CB 153	✓		✓	
CB 180		✓	✓	
<b>PAHs</b>				
Pyr	✓			✓
Phe	✓	✓		
Nap	✓	✓		
Flu	✓	✓		
Fluo	✓		✓	
Acy	✓	✓		
BaP		✓	✓	
IcdP		✓		✓
DahA				✓
BghiP				✓
<b>PBDEs</b>				
BDE 28	✓		✓	
BDE 47		✓	✓	
BDE 99		✓	✓	
BDE 100		✓	✓	
BDE 153		✓		✓
BDE 183		✓		✓
BDE 209			✓	✓

**Table S4** Sensitivity (slope of linear regression) of 4-types SVOCs'  $\Phi$ ,  $\Psi$ , and  $W$  on TSP and precipitation rates

Season Factors	$T \geq 0^\circ\text{C}$ TSP	$U_R$	$T < 0^\circ\text{C}$ TSP	$U_S$
<b>EQ Point (7, 3)</b>				
$\Phi_G$	0%	0%	0%	0%
$\Phi_P$	0%	0%	0%	0%
$\Phi_{R/S}$	0%	0%	0%	0%
$\Psi_{GDD}$	-1%	-41%	-1%	-40%
$\Psi_{PDD} + \Psi_{PWD}$	3%	1%	2%	1%
$\Psi_{GWD}$	-2%	40%	-1%	39%
$\log W_T$	0.02	0.00	0.02	0.00
<b>PR Point (9.64, 6.28)</b>				
$\Phi_G$	-7%	-37%	-7%	-37%
$\Phi_P$	10%	-3%	10%	-3%
$\Phi_{R/S}$	-3%	40%	-3%	40%
$\Psi_{GDD}$	0%	0%	0%	-1%
$\Psi_{PDD} + \Psi_{PWD}$	1%	0%	1%	0%
$\Psi_{GWD}$	-1%	0%	-1%	1%
$\log W_T$	-0.08	0.00	-0.08	0.00
<b>PA Point (10.64, 5.28)</b>				
$\Phi_G$	-34%	-9%	-34%	-9%
$\Phi_P$	38%	-4%	38%	-4%
$\Phi_{R/S}$	-4%	13%	-4%	13%
$\Psi_{GDD}$	0%	-1%	-1%	-4%
$\Psi_{PDD} + \Psi_{PWD}$	33%	0%	33%	0%
$\Psi_{GWD}$	-33%	1%	-32%	4%
$\log W_T$	-0.10	0.00	-0.10	0.00
<b>MP Point (10.64, 6.28)</b>				
$\Phi_G$	-21%	-25%	-21%	-25%
$\Phi_P$	33%	-12%	33%	-12%
$\Phi_{R/S}$	-12%	36%	-12%	36%
$\Psi_{GDD}$	0%	0%	0%	-1%
$\Psi_{PDD} + \Psi_{PWD}$	9%	0%	10%	0%
$\Psi_{GWD}$	-9%	0%	-9%	1%
$\log W_T$	-0.30	0.00	-0.30	0.00

**Table S5** Annual total deposition flux of BDE-209 from 2008 to 2009 in 10 Chinese cities (E: equilibrium; S: steady-state).

Deposition flux ( $\mu\text{g m}^{-2}$ )	Gaseous dry deposition		Particulate deposition (dry and wet)		Gaseous wet deposition		Sum	
	E/S	E	S	E	S	E	S	
Beijing	0.9 (0%/2.3%)	$2.6 \times 10^8$ (99.9%)	6.8 (18.2%)	$1.6 \times 10^5$ (0.1%)	29.5 (79.5%)	$2.6 \times 10^8$	37.2	
Chengdu	0.8 (0%/1.1%)	$3.9 \times 10^7$ (100%)	20.4 (29.2%)	746.2 (0%)	48.7 (69.6%)	$3.9 \times 10^7$	69.9	
Dalian	0.8 (0%/1.6%)	$5.4 \times 10^7$ (100%)	9.5 (19.1%)	329.0 (0%)	39.4 (79.3%)	$5.4 \times 10^7$	49.7	
Harbin	0.8 (0%/2.0%)	$2.3 \times 10^9$ (100%)	4.8 (11.9%)	38755.9 (0%)	34.3 (86.0%)	$2.3 \times 10^9$	39.9	
Kunming	0.4 (0%/0.8%)	$9.8 \times 10^6$ (100%)	7.5 (15.8%)	3170.7 (0%)	39.5 (83.3%)	$9.8 \times 10^6$	47.4	
Lhasa	0.4 (0%/2.7%)	$2.3 \times 10^7$ (99.8%)	1.9 (12.6%)	39631.0 (0.2%)	12.8 (84.7%)	$2.3 \times 10^7$	15.1	
Nanchang	0.2 (0%/0.6%)	$2.0 \times 10^7$ (100%)	3.7 (10.9%)	1954.2 (0%)	30.0 (88.4%)	$2.0 \times 10^7$	33.9	
Shanghai	0.2 (0%/1.4%)	$2.4 \times 10^7$ (100%)	1.9 (15.3%)	571.8 (0%)	10.0 (83.3%)	$2.4 \times 10^7$	12.1	
Shihezi	0.2 (0%/0.6%)	$2.7 \times 10^9$ (99.9%)	4.2 (11.4%)	$3.3 \times 10^6$ (0.1%)	32.1 (88.0%)	$2.7 \times 10^9$	36.5	
Xi'an	0.6 (0%/2.3%)	$9.7 \times 10^7$ (100%)	10.8 (15.8%)	1407.5 (0%)	57.2 (83.4%)	$9.7 \times 10^7$	68.6	

\* We use scientific notation for numbers greater than  $10^5$  to improve readability. The numbers in brackets are the deposition contribution of BDE-209 in each phase of each city.

**Table S6** Comparison between equilibrium models and steady-state models in this study

	Equilibrium models	Our steady-state models
Equations		
$\log K_{PG}$	$\log K_{PG;E} = \log K_{OA} + \log f_{OM} + \log \rho_P - 2.91$ (H-B model)	$\log K_{PG;S} = \log K_{PG;E} + \log \alpha_P$ where, $\log \alpha_P = -\log(1 + 2.27 \times 10^{-11} K_{PG;E})$
$\log K_{RG}$	$\log K_{RG;E} = \log(K_{WA} + 3K_{IA}/r_R)$ (L-W model)	$\log K_{RG;S} = \log K_{RG;E} + \log \alpha_R$ where, $\log \alpha_R = -\log(1 + 5.28 \times 10^{-7} K_{RG;E})$
$\log K_{SG}$	$\log K_{SG;E} = \log K_{JA} + \log S_A \rho_W$ (L-W model)	$\log K_{SG;S} = \log K_{SG;E} + \log \alpha_S$ where, $\log \alpha_S = -\log(1 + 5.28 \times 10^{-7} K_{SG;E})$
Parameters		
$\log K_{PG}$	$K_{OA}$ , $f_{OM}$ , and $\rho_P$	$K_{OA}$ , $f_{OM}$ , and $\rho_P$
$\log K_{RG}$	$K_{WA}$ , $K_{IA}$ , and $r_R$	$K_{WA}$ , $K_{IA}$ , and $r_R$
$\log K_{SG}$	$K_{JA}$ , $S_A$ , and $\rho_W$	$K_{JA}$ , $S_A$ , and $\rho_W$
Upper limits	No theoretical values, but experience values 12 for $\log K_{PG}$ and 6 for $\log K_{RG(SG)}$ was given by L-W model.	10.64 for $\log K_{PG}$ and 6.28 for $\log K_{RG(SG)}$
CSMs	Equilibrium domain (ED)	Steady-state domain (SD)
SVOCs categories	None	EQ, PR, PA, and MP types
Upper limits for scavenging ratios	No	$10^{6.1}$
Predict accuracy	Good for LMW-SVOCs, but overestimate HMW-SVOCs	Good for most SVOCs.

## Text

**Text S1** Clarification of some concepts about partition ratio

### Text S1.1 Particle-gas partition ratio

Here gives the derivation of **Eq. 1** in the manuscript. According to the definition,

$$K_{PG;E} = C_{P;E}/C_{G;E} \quad (S1)$$

$$K_{PE} = C'_{P;E}/(TSP C_{G;E}) \quad (S2)$$

From **Eq. S1-2**, we can calculate dimensionless particle-gas partition ratio ( $K_{PG;E}$ ) and particle-gas partition ratio under equilibrium  $K_{PE}$  values based on obversed data. However, these values can also be calculated from basic parameters:<sup>25</sup>

$$\log K_{PE} = \log K_{OA} + \log f_{OM} - 11.91 \quad (S3)$$

Known that  $C'_{P;E}/C_{P;E} = v_P$  and  $TSP/C_{G;E} = 10^9 \rho_P$ . Thus,

$$\log K_{PG;E} = \log K_{PE} + \log \rho_P + 9 \quad (S4)$$

### Text S1.2 Rain-gas partition ratio and snow-gas partition ratio

Rain-gas partition ratio ( $\log K_{RG;E}$ ) and snow-gas partition ratio ( $\log K_{SG;E}$ ) under equilibrium can be calculated by the definition as

$$\log K_{RG;E} = C_{R;E}/C_{G;E} \quad (S5)$$

$$\log K_{SG;E} = C_{S;E}/C_{G;E} \quad (S6)$$

## Text S2 Relationship between $v_P$ and TSP, $v_W$ and $U_W$

According to the definition, TSP has a linear relationship with  $v_P$ .

$$v_P = \text{TSP}/\rho_P \quad (\text{S7})$$

According to some previous studies,<sup>1,26</sup> we assume the relationship between raindrops and snowflakes radius and their terminal velocities as

$$u_R = 300\sqrt{r_R} \quad (\text{S8a})$$

$$u_S = 22\sqrt{r_S} \quad (\text{S8b})$$

Bringing in  $r_R$  and  $r_S$  from **Table S1**, we have  $u_R = 3$  m/s and  $u_S = 1$  m/s.

Assuming water is uniformly distributed in the atmosphere, we can write two simplified equations. The volume fraction of water in air in rain,  $v_R$  is related to the instantaneous rain rate  $U_R$  as

$$v_R = U_R/u_R \quad (\text{S9a})$$

where  $u_R$  is the averaged raindrop falling velocity.

The volume fraction of water in air in snow,  $v_S$  is related to the instantaneous snow rate  $U_S$  as

$$v_S = U_S/u_S \quad (\text{S9b})$$

where  $u_S$  is the averaged snowflake falling velocity.

Assuming  $v_R = v_S = 3 \times 10^{-7}$ , we have  $U_R = 3.2 \times 10^{-3}$  m h<sup>-1</sup> and  $U_S = 1.1 \times 10^{-3}$  m h<sup>-1</sup>.

## Text S3 Fugacity based methods calculations

### Text S3.1 Z values

Fugacity capacity ( $\text{mol m}^{-3} \text{ Pa}^{-1}$ ) is used to help describe the concentration of a chemical in a system, and the fugacity capacity of gas is defined as

$$Z_G = 1/RT \quad (\text{S10a})$$

According to the definition, the fraction between  $Z_R$  and  $Z_G$  is the  $K_{RG;E}$ . Thus,  $Z_R$  is given as

$$Z_R = K_{RG;E}Z_G \quad (\text{S10b})$$

Similarly,  $Z_S$  can also be calculated by the product of  $Z_G$  and  $K_{SG}$

$$Z_S = K_{SG;E}Z_G \quad (\text{S10c})$$

### Text S3.2 D values for atmospheric chemicals deposition

When  $t \geq 0^\circ\text{C}$ , gaseous chemicals could be directly absorbed by the soil. But when  $t < 0^\circ\text{C}$ , gaseous chemicals are basically absorbed by the snowpack on the earth. However, for the convenience, a simplified method was chosen to calculate gaseous dry deposition for the temperature above and below the freezing point as

$$D_{GDD} = A_0 k_{GD} Z_G \quad (\text{S11a})$$

When  $t \geq 0^\circ\text{C}$ , the wet deposition is in the form of rain. The wet deposition  $D$  value is given by

$$D_{GRD} = A_0 U_W Z_R \quad (\text{S11b})$$

When  $t < 0^\circ\text{C}$ , the wet deposition is in the form of snow. And,

$$D_{GSD} = A_0 U_W Z_S \quad (\text{S11c})$$

$D_{GRD}$  and  $D_{GSD}$  can be collectively referred to as  $D_{GWD}$ .

Particles with chemical absorbed in it tend to deposit to the land under the influence of gravity. The corresponding  $D$  value is

$$D_{PDD} = A_0 v_P k_{PD} Z_P \quad (\text{S11d})$$

Particles can also be scavenged by wet deposition. The  $D$  value of particle wet deposition is given as

$$D_{PWD} = A_0 W_P v_P U_W Z_P \quad (\text{S11e})$$

### Text S3.3 Chemical diffusion between gas and other phases: the mass transfer coefficients (MTCs)

#### *Text S3.3.1 Diffusion between gas and particle*

The diffusion between gaseous and particulate SVOCs mainly follows the absorption process.<sup>27</sup> Li et al. estimated the mass transfer coefficients (MTCs) between gas and particle.<sup>28</sup>

$$k_{PG} = CB_a/l_a \quad (S12)$$

#### *Text S3.3.2 Transfer between gas and raindrop*

We found two different methods to calculate the transfer rate between gas and raindrop, “two-film theory”<sup>1,29</sup> and “one-film theory”<sup>30</sup>. The difference between these two theories is that the two-film theory calculates the rate of absorption inside the raindrop but the one-film theory calculates the rate of adsorption on the raindrop surface. Undoubtedly, the step of transferring from raindrop surface to raindrop inside can limit the overall rate. However, adsorption also makes sense in rain-gas partition process, especially for the HMW chemicals.<sup>1</sup> Also, only HMW SVOCs show obvious difference between steady-state and equilibrium. Thus, we choose the “one-film theory” to calculate the transfer between gas and raindrop. The air side air-raindrop mass transfer coefficient ( $k_{GR}$ ).

$k_{GR}$  should be calculated using an empirical equation<sup>1</sup>

$$k_{GR}(\text{m s}^{-1}) = \left( \frac{D_g}{2r_R} \right) \left[ 2 + 0.6 \left( \frac{v_a}{D_g} \right)^{\frac{1}{3}} \left( \frac{r_R v_R}{v_a} \right)^{\frac{1}{2}} \right] \quad (S13)$$

Bringing in default parameters,  $k_{GR} = 681 \text{ m h}^{-1}$ . Then, we apply the fugacity method.

$$D_{GR} = A_{GR} k_{GR} Z_G \quad (S14)$$

where,

$$A_{GR} = 3hA_0 v_W / r_R \quad (S15)$$

#### *Text S3.3.3 Transfer between gas phase and snowflake phase*

The mass transfer process between air and falling snowflakes has not been studied. Here, we follow the analog of the rain-gas transfer process. The transfer between gas phase and snowflake phase can be treated as a pure adsorption process. Thus, the process only happens on the gas film. Here, we assume that snowflakes are

aerodynamically spherical.  $k_{GS}$  is

$$k_{GS}(\text{m s}^{-1}) = \left( \frac{D_g}{2r_s} \right) \left[ 2 + 0.6 \left( \frac{v_a}{D_g} \right)^{\frac{1}{3}} \left( \frac{r_s v_s}{v_a} \right)^{\frac{1}{2}} \right] \quad (\text{S16})$$

Substituting in the default numbers,  $k_{GS} = 68.3 \text{ m h}^{-1}$

Thus, the  $D$  value is given by

$$D_{GS} = A_{GS} k_{GS} Z_G \quad (\text{S17})$$

Similar with rain, the ratio between  $A_{GS}$  and  $A_0$  can be expressed as<sup>31</sup>

$$A_{GS} = S A_S A_0 \rho_W v_W h \quad (\text{S18})$$

### Text S3.4 Steady-state derivation

#### *Text S3.4.1 Derivation of raindrop-gas partition*

First, under fugacity approach, **Eq. 7** in the main text is

$$f_G D_{GR} = f_R D_{RG} + f_R D_{GRD} \quad (\text{S19})$$

where,  $D_{GR} = D_{RG}$ .

Next, we introduce a value  $\alpha_R$  to represent the difference between raindrops' fugacity and gaseous fugacity under steady-state. According to **Eq. S19**,  $\alpha_R$  should be given as

$$\alpha_R = f_R / f_G = D_{GR} / (D_{RG} + D_{GRD}) \quad (\text{S20})$$

$$\log \alpha_R = -\log \left( 1 + D_{GRD} / D_{GR} \right) \quad (\text{S21})$$

Substituting **Eq. S9a**, **Eq. S11b**, **Eq. S14**, and **Eq. S15**, we get

$$\log \alpha_R = -\log \left( 1 + \frac{A_0 U_R Z_R}{A_{GR} k_{GR} Z_G} \right) = -\log \left( 1 + \frac{u_R r_R Z_R}{3h k_{GR} Z_G} \right) \quad (\text{S22})$$

In the **Eq. S22**,  $Z_R / Z_G = \log K_{RG}$ . Substituting in the default values in **Table S1**, we get **Eq. 8b** in the main text.

The non-equilibrium coefficient  $\alpha_R$  can also represent the difference between equilibrium and non-equilibrium. The deduction is given as

$$\begin{aligned} K_{RG;S} / K_{RG;E} &= (C_{R,S} / C_{G,S}) / (C_{R,E} / C_{G,E}) \\ &= (f_{R,S} / f_{G,S}) / (f_{R,E} / f_{G,E}) \end{aligned} \quad (\text{S23})$$

where, the subscripts E and S represent equilibrium and steady-state respectively.

According to the definition,  $f_{R,E} = f_{G,E}$ . Thus,

$$K_{RG;S} / K_{RG;E} = f_{R,S} / f_{G,S} = \alpha_R \quad (\text{S24})$$

The equation can be written in a log form, that is the **Eq. 8a** in the main text.

$$\log K_{RG,S} = \log K_{RG,E} + \log \alpha_R \quad (S25)$$

*Text S3.4.2 Derivation of snowflake-gas partition*

Similarly, we list the mass balance of snowflake. Under fugacity approach, it is

$$\begin{aligned} N_{G-S} &= N_{S-G} + N_{S-D} \\ f_G D_{GS} &= f_S D_{SG} + f_S D_{GSD} \end{aligned} \quad (S26)$$

where  $D_{SG} = D_{GS}$ .

Similarly, we introduce the snowflake-gas partition non-equilibrium  $\alpha_S$  as the fugacity ratio of snowflake phase and gas phase under steady-state.

$$\alpha_S = f_S / f_G = D_{SG} / (D_{GS} + D_{GSD}) \quad (S27)$$

Substituting **Eq. S9b**, **Eq. S11c**, **Eq. S16**, and **Eq. S18**, we get

$$\log \alpha_S = -\log \left( 1 + \frac{A_0 U_S Z_S}{A_{GS} k_{SG} Z_G} \right) = -\log \left( 1 + \frac{u_S Z_S}{S A_S \rho_W h k_{GS} Z_G} \right) \quad (S28)$$

Then, we have **Eq. 9b** in the main text. Similarly, the **Eq. S29** can also be written in a log form (**Eq. 9a**)

$$\log K_{SG,S} = \log K_{SG,E} + \log \alpha_S \quad (S29)$$

## Text S4 Uncertainty and sensitivity analysis

### Text S4.1 Uncertainty analysis for $\alpha_R$ and $\alpha_S$

In the main text. The different coefficients in  $\alpha_R$  ( $5.29 \times 10^{-7}$ ) and  $\alpha_S$  ( $5.27 \times 10^{-7}$ ) are given with uncertainty range. Their uncertainty ranges are calculated using Oracle® Crystal Ball, respectively. While the  $\alpha_P$  was derived in a previous publication,<sup>28</sup> whose uncertainty analysis is beyond the scope of this study.

The coefficient in  $\alpha_R$  ( $5.29 \times 10^{-7}$ ) has a large uncertainty on  $r_R$  because  $r_R$  is not only the parameter for directly calculating the coefficient (Eq. S22), but  $k_{GR}$  and  $u_R$  are also both functions of  $r_R$  (Eq. S8a&S13). In contrast, other parameters are basically some default constants. If we assume  $r_R$  has the distribution modeled using a three-parameter lognormal distribution (location =  $5 \times 10^{-5}$ , mean =  $1 \times 10^{-4}$ , 95th percentile =  $3 \times 10^{-4}$ ) in Crystal Ball software. It seems to be a low assumption, however, considering the partitioning between gas and drizzle (fog, cloud droplets), it is actually a reasonable assumption.<sup>3</sup> After a Monte-Carlo run for 1,000 samples, the coefficient shows a right-skewed distribution (skewness = 6.73) with elevated kurtosis (62.10), and central 80% uncertainty range from  $4.74 \times 10^{-8}$  to  $1.94 \times 10^{-6}$ .

Similarly, the coefficient in  $\alpha_S$  ( $5.27 \times 10^{-7}$ ) is also uncertain on the dynamic  $r_S$ , which influence the  $k_{GR}$  and  $u_S$ . In Crystal Ball software, considering graupel and snow clumps, we modelled the distribution of  $r_S$  as another three-parameter lognormal distribution (location =  $5 \times 10^{-5}$  m, mean =  $2 \times 10^{-3}$  m, 95th percentile =  $5 \times 10^{-3}$  m). After a Monte-Carlo run for 10,000 samples, we found that the coefficient in  $\alpha_S$  also follow a right-skewed distribution (skewness = 2.14) with elevated kurtosis (10.89) with central 80% uncertainty range from  $1.95 \times 10^{-7}$  to  $9.70 \times 10^{-7}$ .

### Text S4.2 Sensitivity analysis for $\Phi$ , $\Psi$ , and $W$

From the qualitative sensitivity analysis in main text, we can find is a logarithmic relationship between factors (TSP and precipitation rates) and dependent variables ( $\Phi$ ,  $\Psi$  and  $W$ ). Here the Monte-Carlo sensitivity analysis is performed with R language with 50,000 sample size. TSP is assumed to be a log-normal distribution (5th percentile =  $1.5 \mu\text{g m}^{-3}$  and 95<sup>th</sup> percentile =  $150 \mu\text{g m}^{-3}$ ), so are  $U_R$  (5th percentile =  $3.2 \times 10^{-4} \text{ m h}^{-1}$  and 95<sup>th</sup> percentile =  $3.2 \times 10^{-2} \text{ m h}^{-1}$ ) and  $U_S$  (5th percentile =  $1.1 \times 10^{-4} \text{ m h}^{-1}$  and 95<sup>th</sup> percentile =  $1.1 \times 10^{-2} \text{ m h}^{-1}$ ). The sensitivity is defined as the slope of linear regression between  $\Phi$ ,  $\Psi$ , and  $W$  and normalized logarithm TSP and precipitation rates, which

have same units as  $\Phi$ ,  $\Psi$ , and  $W$ .

### **Text S4.3 Discussion on unquantified uncertainty factors**

Besides the uncertainty and sensitivity analysis mentioned above, as a simulation of field monitoring, this study still has some uncertainties that cannot be quantified.

#### *Text S4.3.1 The uncertainty of Antoine parameters ( $A_{XY}$ , $B_{XY}$ )*

Antoine parameters (**Table S2**) are critical parameters in calculating basic partition ratios ( $K_{OA}$ ,  $K_{WA}$ ) and adsorption coefficients ( $K_{IA}$  and  $K_{SA}$ ). These values were collected and organized by a previous study,<sup>4</sup> and would have the following uncertainty influencing the steady-state equations (1) The two-parameter Antoine equation (**Eq. 5**) does not consider inner energy changes are also functions of temperature; (2) The performance of pp-LFERs equations and parameters may vary on different chemicals. The accuracy may not be satisfactory for some substances.

These parameters may influence the values of partition ratios, but they will **not** influence the relationship between partition ratios under equilibrium and steady-state (**Eq. 6b, 8b, and 9b**).

#### *Text S4.3.2 The uncertainty of environmental “constants”*

In the deviation of steady-state partition ratios, there are some environmental properties such as deposition rates ( $k_{PG}$  and  $k_{GD}$ ), specific area of snowflake ( $SAs$ ), and kinematic viscosity of air ( $\nu_a$ ),<sup>2</sup> which are generally assumed to be constant in environmental studies. Although their changes may have some impact on the model, the impact is limited due to the limited range of changes of these variables.

#### *Text S4.3.3 The uncertainty of monitoring data*

Measurement records play an important role in validating the steady-state model of this study. However, measurements themselves may have a certain degree of uncertainty according to equipment and analytical methods, which may blur the phenomena.

In addition, measurements in this study were collected from different databases and papers. Comparing the measurement results of different methods will also produce certain uncertainties.

#### *Text S4.3.4 The uncertainties in case studies*

In this study, we performed three case studies in real-world to show the differences between steady-state theory and equilibrium theory and the broad application prospects of steady-state partitioning theory. The uncertainties of case studies come from two aspects.

Uncertainty from the steady-state equations. In **Fig. 1**, the main text, we show the uncertainties of steady-state rain-gas and snow-gas partition equations, which influence the effect of steady-state deviating from equilibrium. The weaker this effect is, the closer the steady-state theory is to equilibrium. Discuss separately, in case 1, if the effect is weaker than estimated,  $\beta$ -HCH's CTD under steady-state will be smaller and closer to equilibrium, and vice versa. In case 2, if the effect is weaker than estimated, the global distribution under steady state will not be as uniform as it is now, but will be closer to that under equilibrium, and vice versa. However, as a PA-Type SVOC, CB-180 has a certain distance from the upper limit of  $\log K_{RG;S}$  and  $\log K_{SG;S}$ . Therefore, the uncertainty of case 2 is relatively weak. In case 3, if the effect is weaker than estimated, the annual deposition flux of BDE-209 under steady state will be much larger and much closer to that under equilibrium, and vice versa.

Uncertainty from TSP and precipitation rates. TSP and precipitation can directly influence SVOCs' distribution, deposition, and scavenging, but will not directly change the difference between steady-state and equilibrium partitioning. In case 1, as a PR-Type SVOC,  $\beta$ -HCH's distribution is sensitive to  $U_S$  ([Table S4](#)). Therefore, if  $U_S$  is larger than estimated, the long-range atmospheric transport of  $\beta$ -HCH will be weakened both under steady state and equilibrium, and vice versa. In case 2, as a PA-Type SVOC, CB-180 is sensitive to TSP ([Table S4](#)). Therefore, if TSP is larger than estimated, the global distribution of CB-180 will be hindered both under steady state and equilibrium, and vice versa. In case 3, as a MP-Type SVOC, BDE-209 is both sensitive to TSP and  $U_R/U_S$  ([Table S4](#)). Therefore, if TSP and  $U_R/U_S$  are larger than estimated, the annual deposition flux of BDE-209 in Chinese cities will increase both under steady state and equilibrium, and vice versa.

## **Text S5 Methods of case studies**

### **Text S5.1 OECD POV & LRTP Screening Tool on $\beta$ -HCH**

The OECD POV & LRTP Screening Tool is a freely available, consensus-based multimedia model software designed to assess the environmental persistence (POV) and long-range transport potential (LRTP) of non-ionizing organic chemicals.<sup>32</sup> Characteristic Travel Distance (CTD) is defined as a transport-oriented LRTP indicator. It quantifies the distance a chemical travel from its point of release to the point where its concentration drops to  $1/e$  (approximately 37%) of its initial value.

Based on this model, we made some modifications to fit the Arctic environment as assumed in this case study.

- Temperature was set to -15 °C.
- Arctic area was set to  $2.13 \times 10^{13} \text{ m}^2$ , where  $1.34 \times 10^{13} \text{ m}^2$  was set to water.<sup>33</sup>
- Rain scavenging was changed to snow scavenging. And we set  $U_S = 1.25 \times 10^{-5} \text{ m h}^{-1}$ , and  $\text{TSP} = 10 \mu\text{g m}^{-3}$  as a typical polar environment.<sup>33</sup>
- Partition ratios of  $\beta$ -HCH was set same as this study, while the half-lives of  $\beta$ -HCH are collected from a publications<sup>33</sup> as 2127 h in air, 5250 h in water, and 21000 h in soil at 25°C.

### **Text S5.2 BETR Global V2.0 model**

BETR Global is a multimedia chemicals' fate model downloaded from <https://sites.google.com/site/betrglobal/downloads>.<sup>34</sup> It divides the global environment into 288  $15^\circ \times 15^\circ$  grid cells; in each grid, the model simulates concentrations within, and transport between, seven compartments including upper air, lower air, vegetation, soil, freshwater, freshwater sediment, and ocean water. Here, we run the model for CB-180 from 1960 to 2019 and get the results in 2019 after 60-years globally transport. The input parameters are all set as the default values in the model.

### **Text S5.3 Calculation of BDE-209's annual total deposition**

The calculation process of BDE-209's annual total deposition is listed below.

**Step 1**, gaseous BDE-209 concentration values were measured by SAMP-II from September 2008 to August 2009.<sup>8</sup> The TSP values were measured by SAMP-II and precipitation rates and types were obtained from the Open-Meteo (<https://open-meteo.com>)

[meteo.com/](http://meteo.com/)).

**Step 2**, the deposition rate during sampling ( $\mu\text{g m}^{-2} \text{ day}^{-1}$ ) is calculated with Lei and Wania's approach,<sup>2</sup> which has been used in calculating deposition contribution (**Table 1**).

$$\text{Gaseous dry deposition} = C_G k_{GD} \quad (\text{S30a})$$

$$\text{Gaseous wet deposition} = C_G U_W K_{RG/SG} \quad (\text{S30b})$$

$$\text{Particulate deposition (dry + wet)} = C_G v_P (k_{PD} + W_P U_W) \quad (\text{S30c})$$

**Step 3**, the nearest neighbor interpolation (R language, zoom.na.locf function) was used to fill gaps in the whole year.

**Step 4**, we summed each deposition flux over a year ( $\mu\text{g m}^{-2}$ ) to acquire annual total deposition value.

**Text S6** Vapor pressure based and octanol-air based absorptive partitioning approaches

### Text S6.1 Junge-Pankow model

The Junge-Pankow (J-P)<sup>35</sup> model was originally suggested by Junge and later critically reviewed by Pankow, assuming the SVOCs are entirely adsorbed onto the surface of particle matters. The particulate phase fraction ( $\phi_P$ ) in the J-P model could be calculated by

$$\phi_P = \frac{C_J \theta}{C_J \theta + P_L} \quad (\text{S31})$$

where  $\theta$  (cm<sup>2</sup><sub>surface</sub> cm<sup>-3</sup><sub>air</sub>) is the particle surface area concentration.  $C_J$  (Pa cm) is based on the heat of desorption from the particle surface, the heat of vaporization of the compound, and the moles of adsorption sites on the aerosol. The  $P_L$  (Pa) is the sub-cooled liquid vapor pressure, which is a function of temperature  $T$  (K).

Pankow et al.<sup>35</sup> derived the equations to describe the G/P partitioning of SVOCs based adsorption mechanism,

$$K_{PE} = \frac{N_S A_{TSP} T e^{(Q_1 - Q_v)/RT}}{1600 P_L^0} \quad (P_L^0 \text{ in torr}) \quad (\text{S32})$$

and late the equation based on both adsorption and absorption mechanism.<sup>36</sup>

$$K_{PE} = \frac{1}{P_L^0} \left[ \frac{N_S A_{TSP} T e^{(Q_1 - Q_v)/RT}}{1600} + \frac{760 f_{OM} RT}{MW_{OM} \zeta_{OM} 10^6} \right] \quad (P_L^0 \text{ in torr}) \quad (\text{S33})$$

where  $f_{OM}$  is the fraction of the particle mass that consists of absorbing organic matter having molecular weight  $M_{OM}$  (g mol<sup>-1</sup>) and activity coefficient  $\zeta_{OM}$  in the organic film.

Then, an absorption mechanism for gas-particle partitioning of SVOCs was described in relation to the chemical octanol-air partition coefficient,  $K_{OA}$  (unitless), by Finizio et al.<sup>37</sup>

$$\log K_{PE} = \log K_{OA} + \log \frac{1.22 \times 10^{-12} f_{OM} MW_{OCT} \zeta_{OCT}}{MW_{OM} \zeta_{OM}} \quad (\text{S34})$$

where  $\zeta_{OCT}$  is the activity coefficients of the absorbing compound in octanol,  $MW_{OCT}$  is the molecular weights of octanol.

Later, Pankow modified the absorption equation<sup>38</sup>

$$\log K_{PE} = \log K_{OA} + \log \frac{\zeta_{OCT}}{\zeta_{OM}} + \log \frac{f_{OM} MW_{OCT}}{10^{12} MW_{OM} \rho_{OCT}} \quad (\text{S35})$$

where,  $\rho_{OCT}$  is the density of octanol.

### Text S6.2 Harner-Bidleman model

With the assumptions that  $\zeta_{\text{OCT}}/\zeta_{\text{OM}}$  and  $MW_{\text{OCT}}/MW_{\text{OM}} = 1$ , Harner and Bidleman<sup>25</sup> derived an absorption equation under equilibrium condition to calculate  $K_{\text{P}}$ , given by

$$\log K_{\text{PE}} = \log K_{\text{OA}} + \log f_{\text{OM}} - 11.91 \quad (\text{S36})$$

The  $K_{\text{OA}}$  absorption model can be used to predict values of  $K_{\text{P}}$  from knowledge of only  $K_{\text{OA}}$  and the organic fraction of the aerosol,  $f_{\text{OM}}$ , if it is further assumed that all of the aerosol organic matter is available to absorb gaseous compounds.

### Text S6.3 Comparison between pressure based and octanol-air based absorptive partitioning equations

Both pressure based and octanol-air based absorptive partitioning equations have made significant contributions in studying the P/G partitioning processes of SVOCs in the atmosphere.

While both  $P_{\text{L}}$  and  $K_{\text{OA}}$  can be used to predict G/P partition of SVOCs, predictability based on the two parameters is about the same. Xiao and Wania<sup>39</sup> compiled and evaluated a large dataset of  $P_{\text{L}}$  and  $K_{\text{OA}}$  for several sets of non-polar SVOCs, including PBDEs, and concluded that it is impossible to judge one parameter being better than the other. This is because  $P_{\text{L}}$  and  $K_{\text{OA}}$  obtained at the same temperature for any given compound are strongly correlated as given by<sup>40</sup>

$$\log K_{\text{OA}} = -\log P_{\text{L}} + 6.46 \quad (\text{S37})$$

As suggested by Harner and Bidleman,<sup>25</sup> a problem with the absorption model (**Eq. S34**) is that  $\zeta_{\text{OM}}$  is not often known and may vary substantially among different classes of compounds.<sup>41,42</sup> The  $K_{\text{OA}}$  absorption model (**Eq. S35**), however, requires knowledge of only  $K_{\text{OA}}$  and the organic matter fraction of the aerosol which are both more easily measurable than the parameters of the Junge–Pankow model.

We prefer to use the parameter  $K_{\text{OA}}$  here, since it works together with  $K_{\text{WA}}$ ,  $K_{\text{IA}}$ , and  $K_{\text{JA}}$  can reflect the chemicals' volatility in different solvents or on different adsorption surfaces (particle, rain, and snow), compared with  $P_{\text{L}}$ . We would like to point out that both  $P_{\text{L}}$ - and  $K_{\text{OA}}$ -based models mentioned above are developed under equilibrium theory. Comparison between these two equations and other five with the steady-state model<sup>28</sup> have been made by Qiao and co-workers<sup>6</sup>.

## Reference

1. Simcik, M. F. The importance of surface adsorption on the washout of semivolatile organic compounds by rain. *Atmospheric Environment* **38**, 491–501 (2004).
2. Lei, Y. D. & Wania, F. Is rain or snow a more efficient scavenger of organic chemicals? *Atmospheric Environment* **38**, 3557–3571 (2004).
3. Seinfeld, J. H. & Pandis, S. N. *Atmospheric Chemistry and Physics: From Air Pollution to Climate Change.* (2016).
4. Yang, P.-F. *et al.* Temperature dependence of the rain-gas and snow-gas partition coefficients for nearly a thousand chemicals. *Chemosphere* **142565** (2024) doi:10.1016/j.chemosphere.2024.142565.
5. Indiana University. Integrated Atmospheric Deposition Network (IADN) Data Visualization Tool. IADN Data Viz (2024).
6. Qiao, L.-N. *et al.* Modeling gas/particle partitioning of polybrominated diphenyl ethers (PBDEs) in the atmosphere: A review. *Science of The Total Environment* **729**, 138962 (2020).
7. Noël, M. *et al.* Do trans-Pacific air masses deliver PBDEs to coastal British Columbia, Canada? *Environmental Pollution* **157**, 3404–3412 (2009).
8. Yang, M. *et al.* Polybrominated Diphenyl Ethers in Air across China: Levels, Compositions, and Gas-Particle Partitioning. *Environ. Sci. Technol.* **47**, 8978–8984 (2013).
9. Mariani, G. *et al.* Atmospheric input of POPs into Lake Maggiore (Northern Italy): PBDE concentrations and profile in air, precipitation, settling material and sediments. *Chemosphere* **73**, S114–S121 (2008).
10. Liu, J. *et al.* Diurnal and nocturnal variations of PAHs in the Lhasa atmosphere, Tibetan Plateau: Implication for local sources and the impact of atmospheric degradation processing. *Atmospheric Research* **124**, 34–43 (2013).
11. Wang, Z. *et al.* Gas/particle partitioning of polycyclic aromatic hydrocarbons in coastal atmosphere of the north Yellow Sea, China. *Environ Sci Pollut Res* **20**, 5753–5763 (2013).
12. Zhang, L. *et al.* Assessment of halogenated POPs and PAHs in three cities in the Yangtze River Delta using high-volume samplers. *Science of The Total Environment* **454–455**, 619–626 (2013).
13. Zhao, J., Zhang, F., Chen, J. & Xu, Y. Characterization of polycyclic aromatic

- hydrocarbons and gas/particle partitioning in a coastal city, Xiamen, Southeast China. *Journal of Environmental Sciences* **22**, 1014–1022 (2010).
14. Ma, W.-L. *et al.* Seasonal variations of sources of polycyclic aromatic hydrocarbons (PAHs) to a northeastern urban city, China. *Chemosphere* **79**, 441–447 (2010).
  15. Ma, W.-L. *et al.* Implications for long-range atmospheric transport of polycyclic aromatic hydrocarbons in Lhasa, China. *Environ Sci Pollut Res* **20**, 5525–5533 (2013).
  16. Ma, Y. *et al.* Deposition of polycyclic aromatic hydrocarbons in the North Pacific and the Arctic. *Journal of Geophysical Research: Atmospheres* **118**, 5822–5829 (2013).
  17. Smith, D. J. T. & Harrison, R. M. Concentrations, trends and vehicle source profile of polynuclear aromatic hydrocarbons in the U.K. atmosphere. *Atmospheric Environment* **30**, 2513–2525 (1996).
  18. Ravindra, K. *et al.* Seasonal and site-specific variation in vapour and aerosol phase PAHs over Flanders (Belgium) and their relation with anthropogenic activities. *Atmospheric Environment* **40**, 771–785 (2006).
  19. Mandalakis, M., Tsapakis, M., Tsoga, A. & Stephanou, E. G. Gas–particle concentrations and distribution of aliphatic hydrocarbons, PAHs, PCBs and PCDD/Fs in the atmosphere of Athens (Greece). *Atmospheric Environment* **36**, 4023–4035 (2002).
  20. Ramírez, N., Cuadras, A., Rovira, E., Marcé, R. M. & Borrull, F. Risk Assessment Related to Atmospheric Polycyclic Aromatic Hydrocarbons in Gas and Particle Phases near Industrial Sites. *Environmental Health Perspectives* **119**, 1110–1116 (2011).
  21. Gregoris, E. *et al.* Gas-particle distributions, sources and health effects of polycyclic aromatic hydrocarbons (PAHs), polychlorinated biphenyls (PCBs) and polychlorinated naphthalenes (PCNs) in Venice aerosols. *Science of The Total Environment* **476–477**, 393–405 (2014).
  22. Tsapakis, M. & Stephanou, E. G. Polycyclic Aromatic Hydrocarbons in the Atmosphere of the Eastern Mediterranean. *Environ. Sci. Technol.* **39**, 6584–6590 (2005).
  23. Saha, M. *et al.* Seasonal Trends of Atmospheric PAHs in Five Asian Megacities and Source Detection Using Suitable Biomarkers. *Aerosol Air Qual. Res.* **17**, 2247–

2262 (2017).

24. Wang, X., Gong, P., Sheng, J., Joswiak, D. R. & Yao, T. Long-range atmospheric transport of particulate Polycyclic Aromatic Hydrocarbons and the incursion of aerosols to the southeast Tibetan Plateau. *Atmospheric Environment* **115**, 124–131 (2015).
25. Harner, T. & Bidleman, T. F. Octanol–Air Partition Coefficient for Describing Particle/Gas Partitioning of Aromatic Compounds in Urban Air. *Environ. Sci. Technol.* **32**, 1494–1502 (1998).
26. Loftus, K. & Wordsworth, R. D. The Physics of Falling Raindrops in Diverse Planetary Atmospheres. *Journal of Geophysical Research: Planets* **126**, e2020JE006653 (2021).
27. Li, Y.-F., Qiao, L.-N., Ren, N.-Q., Macdonald, R. W. & Kannan, K. Gas/particle partitioning of semi-volatile organic compounds in the atmosphere: Transition from unsteady to steady state. *Science of The Total Environment* **710**, 136394 (2020).
28. Li, Y. F., Ma, W. L. & Yang, M. Prediction of gas/particle partitioning of polybrominated diphenyl ethers (PBDEs) in global air: A theoretical study. *Atmospheric Chemistry and Physics* **15**, 1669–1681 (2015).
29. Tsai, W., Cohen, Y., Sakugawa, H. & Kaplan, I. R. Dynamic partitioning of semivolatile organics in gas/particle/rain phases during rain scavenging. *Environ. Sci. Technol.* **25**, 2012–2023 (1991).
30. Seinfeld, J. H. & Pandis, S. N. *Atmospheric Chemistry and Physics: From Air Pollution to Climate Change*. (J. Wiley, Hoboken, N.J, 2006).
31. Stocker, J., Scheringer, M., Wegmann, F. & Hungerbühler, K. Modeling the Effect of Snow and Ice on the Global Environmental Fate and Long-Range Transport Potential of Semivolatile Organic Compounds. *Environ. Sci. Technol.* **41**, 6192–6198 (2007).
32. Wegmann, F., Cavin, L., MacLeod, M., Scheringer, M. & Hungerbühler, K. The OECD software tool for screening chemicals for persistence and long-range transport potential. *Environmental Modelling & Software* **24**, 228–237 (2009).
33. Yang, P.-F. *et al.* Modeling historical budget for  $\beta$ -Hexachlorocyclohexane (HCH) in the Arctic Ocean: A contrast to  $\alpha$ -HCH. *Environ Sci Ecotech* **14**, 100229 (2023).
34. MacLeod, M. *et al.* BETR global – A geographically-explicit global-scale multimedia contaminant fate model. *Environmental Pollution* **159**, 1442–1445

(2011).

35. Pankow, J. F. Review and comparative analysis of the theories on partitioning between the gas and aerosol particulate phases in the atmosphere. *Atmospheric Environment* (1967) **21**, 2275–2283 (1987).
36. Pankow, J. F. An absorption model of gas/particle partitioning of organic compounds in the atmosphere. *Atmospheric Environment* **28**, 185–188 (1994).
37. Finizio, A., Mackay, D., Bidleman, T. & Harner, T. Octanol-air partition coefficient as a predictor of partitioning of semi-volatile organic chemicals to aerosols. *Atmospheric Environment* **31**, 2289–2296 (1997).
38. Pankow, J. F. Further discussion of the octanol/air partition coefficient  $K_{oa}$  as a correlating parameter for gas/particle partitioning coefficients. *Atmospheric Environment* **32**, 1493–1497 (1998).
39. Xiao, H., Li, N. & Wania, F. Compilation, Evaluation, and Selection of Physical-Chemical Property Data for  $\alpha$ -,  $\beta$ -, and  $\gamma$ -Hexachlorocyclohexane. *J. Chem. Eng. Data* **49**, 173–185 (2004).
40. Yang, M., Li, Y.-F., Qiao, L.-N. & Zhang, X.-M. Estimating subcooled liquid vapor pressures and octanol-air partition coefficients of polybrominated diphenyl ethers and their temperature dependence. *Science of The Total Environment* **628–629**, 329–337 (2018).
41. Liang, C. & Pankow, J. F. Gas/Particle Partitioning of Organic Compounds to Environmental Tobacco Smoke: Partition Coefficient Measurements by Description and Comparison to Urban Particulate Material. *Environ. Sci. Technol.* **30**, 3650–3650 (1996).
42. Jang, M., Kamens, R. M., Leach, K. B. & Strommen, M. R. A Thermodynamic Approach Using Group Contribution Methods to Model the Partitioning of Semivolatile Organic Compounds on Atmospheric Particulate Matter. *Environ. Sci. Technol.* **31**, 2805–2811 (1997).